Published online January 18, 2018

Original Research

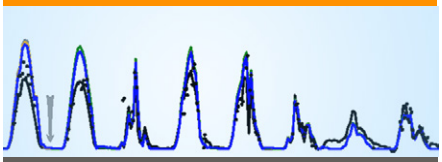

Core Ideas

- Detailed description of plant growth dynamics improves heat flux simulations.
- Harvest cannot be neglected to adequately simulate boundary layer energy fluxes.
- Complex plant growth models improve flux exchanges under drought conditions.

C. Klein, C. Biernath, F. Heinlein, C. Thieme, and E. Priesack, Helmholtz Zentrum München, German Research Center for Environmental Health, Institute of Biochemical Plant Pathology, Modeling Soil–Plant–Atmosphere Systems, Ingolstädter Landstraße 1, D-85764 Neuherberg, Germany; A.K. Gilgen, ETH Zurich, Institute of Agricultural Sciences, Grassland Sciences, Universitätstraße 2, CH-8092 Zurich, Switzerland; M. Zeeman, Karlsruhe Institute of Technology, IMK-IFU, KIT-Campus Alpin, Kreuzeckbahnstraße 19, D-82467 Garmisch-Partenkirchen, Germany. *Corresponding author (chrikle@web.de).

Received 7 Mar. 2017.
Accepted 5 Nov. 2017.

Citation: Klein, C., C. Biernath, F. Heinlein, C. Thieme, A.K. Gilgen, M. Zeeman, and E. Priesack. 2017. Vegetation growth models improve surface layer flux simulations of a temperate grassland. Vadose Zone J. 16(13). doi:10.2136/vzj2017.03.0052

Vol. 16, Iss. 13, 2017

Vegetation Growth Models Improve Surface Layer Flux Simulations of a Temperate Grassland

Christian Klein,* Christian Biernath, Florian Heinlein, Christoph Thieme, Anna Katarina Gilgen, Matthias Zeeman, and Eckart Priesack

Grassland models represent interactions of plant growth with soil and agricultural management based on underlying processes in different degrees of detail. To better understand the impact of these differences on the simulation of energy and matter exchange at the land-surface layer, we compared the ability of five land-surface models with different degrees of complexity to simulate energy fluxes in an intensively managed grassland in Switzerland. The aim was to evaluate the impacts of biomass growth, biomass harvest, soil profile characterization, and rooting depth on the dynamics of simulated near-surface soil moisture contents and energy fluxes. The case study included a comparison of model results with continuous observations of latent heat, sensible heat, and net radiation for a site-year. Energy fluxes were simulated more accurately by including a biomass growth model, encompassing the abrupt decline in leaf area caused by harvest. Site-specific soil parametrization in combination with the absence of restrictions on rooting depth also improved the simulation results. The simulated energy fluxes of the five models differed significantly in the hot, dry month of July 2010 but were negligible under moist conditions in May. We conclude that the application of dynamic vegetation growth models improves energy flux simulations at the field scale in intensively managed grasslands during summer if biomass harvest dates and site-specific soil profile descriptions are considered. Our results imply that regional-scale simulations of grasslands will benefit significantly from high-resolution input information on soil properties, land use, and management.

Abbreviations: LAI, leaf area index; LSM, land surface model; HPM, Hurley Pasture Model; WFPS, water-filled pore space.

Grasslands cover >25% of the Earth's surface area and about 70% of the agricultural land area (FAO, 2015, p. 50). Therefore, a good representation of grassland systems in models plays a crucial role in reliably estimating energy and matter exchange between the land surface and the atmosphere at regional and global scales. During the last decades, increasingly improved terrestrial ecosystem models have been developed and applied to simulate energy, water and C fluxes between biosphere and atmosphere (Ma et al., 2015; Ershadi et al., 2014) and to estimate crop production under expected climate change (Asseng et al., 2013).

However, compared with the numerous accessible forest and crop system models and in spite of the widespread surface area occupied by grassland, only a few grassland-specific models are available (Chang et al., 2013; Ma et al., 2015; Senapati et al., 2016), which for their part additionally address specific research questions. Among others, these are the CENTURY model built to quantify C, N, P, and S turnover on a monthly basis (Parton et al., 1998) and rebuilt for daily time steps under the name DAYCENT, the grassland model GEM (Chen et al., 1996a) focusing on natural grasslands, the LINGRA model (Schapendonk et al., 1998) to particularly predict biomass productivity of perennial ryegrass (*Lolium perenne* L.), the Hurley Pasture Model (HPM) designed to estimate water, C, and N fluxes in grazed soil–pasture systems (Thornley, 1998) and the model PASIM

(Riedo et al., 1998) derived from the HPM to additionally simulate gaseous emissions from the pasture system.

An overview of further grazed pasture system models that consider agricultural management at the whole farm level in contrast to single paddocks was given by Snow et al. (2014), describing the strengths and weaknesses of the models APSIM (Holzworth et al., 2014), AgMod (Johnson, 2013), DIESE (Clouaire and Rellier, 2009), FASSET (Hutchings et al., 2007), GRAZPLAN (Donnelly et al., 2002), and IFSM (Rotz et al., 2013). Similar to the APSIM model platform, further crop models and model platforms such as STICS (Brisson et al., 2003; Ruget et al., 2009), EPIC (Williams et al., 1989), CropSyst (Stöckle et al., 2003), DNDC (Li et al., 1992, 1994), DSSAT (Jones et al., 2003), and Expert-N (Priesack, 2006) have been extended to simulate grassland ecosystems. They strongly contribute to the development of grassland models, often by providing more detailed or different process descriptions including for example soil freezing and thawing, soil water flow in macropores, soil gas transport, and adaption to CO_2 fertilization, although the more detailed process models may for daily time steps need to be parameterized and tested for grassland system simulations. Furthermore, during the last years mainly for crop and grasslands, a better representation of land use management was introduced to global dynamic vegetation models, for example LPjmL (Bondeau et al., 2007; Strengers et al., 2010; Fader et al., 2015), BIOME-BGC (Hidy et al., 2012; Keller et al., 2014), ORCHIDEE-GM (Chang et al., 2013, 2015), and JULES-SUCROS (van den Hoof et al., 2011; Williams and Falloon, 2015).

Land surface models (LSMs) that are implemented in global or regional models for representing the surface layer mostly use simple soil and vegetation models that lack descriptions of dynamic vegetation growth, land-use management, and soil physics. Studies (Song et al., 2013; van den Hoof et al., 2011; Casanova and Judge, 2008) have shown that these model components affect the simulations of soil water content, nutrient availability for plant growth, canopy properties, and plant biomass growth. Falge et al. (2005) determined that vegetation type and the accurate description of leaf physiology is more important to the surface energy balance, which is the most relevant part of a LSM in weather models, than the leaf area index (LAI) of a system. However, they did not discuss the influence of soil types and physical properties. In contrast, Calanca et al. (2016) concluded by simulating managed grassland sites in Switzerland that especially the description of the soil and mechanistic plant growth is very important for simulating droughts. Also, Zeeman et al. (2010) showed that management practices can strongly influence the C fluxes triggered by climate conditions from three grassland sites in Switzerland. Another study confirmed that human activities in steppe ecosystems resulted in a rapid shift between latent and sensible heat and had a strong impact on the C budget (Chen et al., 2009). Even two adjacent grassland fields under different management regimes (fertilization and cutting frequency) can have significantly different C budgets (Ammann et al., 2007).

Land surface models impact the soil water content, canopy height, plant biomass, and soil cover. Thus, simple LSMs might be biased by incompletely describing surface energy fluxes and by neglecting processes that consider water and nutrient availability for plant growth. The impact of growing roots and rooting depth on soil water storage and surface energy fluxes is well known but rarely realized in LSMs. Gayler et al. (2014) therefore analyzed the importance of an adequate representation of crops on surface energy flux simulations. Compared with field crops, the rooting depth of permanent grasslands does not change much throughout the year (Sindhøj et al., 2000; Fiala, 2010). In contrast, the aboveground biomass of grasslands may change rapidly throughout the year due to sudden harvest events and thus affect the site-specific or regional microclimate (Gigante et al., 2009; Zeeman et al., 2010).

Grassland management systems can strongly differ among sites due to different climatic and soil conditions, different species compositions, and different grassland and feed quality requirements. Examples are hay, forage, silage, and bioenergy production, livestock grazing, fallowing, restrictions due to nature protection, or the rapid overgrowth of unmanaged grasslands by trees (Silva et al., 2008). These differences result in varying frequencies of harvest and cutting heights, fertilizer applications, livestock densities, and irrigation and thus affect surface energy fluxes. In spite of these differences, only a few simulation studies have considered the influence of management on water and energy fluxes in grasslands (Fatichi et al., 2014; Kirschbaum et al., 2015).

The objective of this study was therefore to assess the ability of five models with different levels of complexity to simulate energy fluxes in a grassland-dominated region of Switzerland based on flux tower measurements at one intensively managed temperate grassland site in 2006. The applied models were the widely applied LSM Noah (Chen et al., 1996b, 1997; Koren et al., 1999; Chen and Dudhia, 2001; Ek et al., 2003) and four different model configurations of the LSM Expert-N (Priesack et al., 2006; Priesack, 2006; Biernath et al., 2011). We use the Noah model, which was developed as a LSM for the regional scale and which is used in couplings with weather and climate models (Skamarock et al., 2008), as a reference model.

In particular, we assessed the influence of (i) different descriptions of plant growth, (ii) a more site-specific vs. a more general description of soil properties and site-specific harvest management, and (iii) different rooting depths on the simulation results and their relevance to descriptions of flux exchanges.

Materials and Methods

Field Site Description and Underlying Data

The examined field site at Chamau (47°12′37″ N, 8°24′38″ E, 393 m asl) is an intensively managed grassland comprising

approximately 20 grass and herb species in the Swiss Lowlands (Roth 2006).The simulation period covered the entire year 2006 and no fertilizers were applied during this time period. Due to the focus of this work on the effects of plant growth and harvest management on the near-surface flux exchanges, we evaluated the vegetation period from May to August, as well as two extreme periods: a temperate and moist period in May and a hot and dry period in July. Forage was harvested on 4 May, 9 June, 10 July, 5 Sept., and 19 Oct. 2006, with a cutting height of 0.07 m. The species composition, site, experimental design, biomass, and grassland management were described in detail by Gilgen and Buchmann (2009), Roth (2006), and Zeeman et al. (2010). The ecosystem variables relevant for the simulations were used as documented in Gilgen and Buchmann (2009) (plant variables and soil moisture) and Roth (2006) (soil properties). Micrometeorological data were used at 30-min resolution. Fluxes were determined using the eddy covariance technique. It is well-known that eddy covariance tower measurements can have high uncertainties. Zeeman et al. (2010) showed that the energy budget closure amounts to 81% at this site station.

An overview of the soil property data used by the models and the measurement setup is given in Tables 1 and 2, respectively.

Model Approaches

We applied the following LSM systems: (i) the LSM Noah, which was originally developed to simulate the lower boundary conditions for weather forecast and climate research at the global and regional scales (Skamarock et al., 2008); and (ii) the Expert-N model system, which was developed to improve process understanding simulating matter fluxes in terrestrial ecosystems and agricultural consultation. In principle, the modularity of Expert-N permits the establishment of numerous models to analyze the impacts of individual functions and processes on the modeled system and the simulation results. Site-specific conditions can be described in great detail depending on the availability of data. We applied the Noah model (Model I) and four different configurations of Expert-N 5.0 (Models II–V).

Table 1. Description of the physical soil parameters for Model II and five horizons for Models III to V, which were executed in the Expert-N model environment.

Property	Model II†	Models III to V‡				
		A_h	B_v	G_o	G_r	elC_v
Thickness, cm	200	15	20	25	20	50
Numerical layers	40	3	4	5	4	10
Clay, %	18.0	24.4	24.5	25.6	17.2	17.2
Silt, %	39.0	50.2	50.9	24.3	20.5	20.5
Sand, %	43.0	25.4	24.6	50.1	62.3	62.3
Bulk density, g cm^{-3}	1.39	1.11	1.33	1.57	1.57	1.57
Porosity, %	47.7	50.8	41.15	30.53	30.53	30.53
Field capacity, %	38.3	45.8	41.0	30.0	22.1	17.4
Wilting point, %	8.4	15.9	16.9	16.4	8.7	8.14
Sat conductivity, mm d^{-1}	242.8	210	210	100	130	130
Organic matter, %	1.98	7.0	3.0	0.5	0.3	0.1
Rock fraction, %	0.0	0.7	0.9	45.0	55.0	60.0
pH	6.2	5.3	5.2	6.9	7.3	7.8

† Following Cosby et al. (1984) for loam soil type.
‡ Following Roth (2006) for Cambisol soil type.

Model I

The Noah model was applied as documented in Chen et al. (1996b, 1997), Chen and Dudhia (2001), Ek et al. (2003), and Koren et al. (1999) without further modifications. The land-use type "grassland," the soil type "loam," and interpolated LAI dynamics based on the measurements without explicit harvest management were used. The loam soil type, which was described by Miller and White (1998), was the soil class that best represented the measured topsoil horizon parameters at Chamau (Roth, 2006). The 200-cm soil profile comprised four horizons with uniform soil properties. The predefined rooting depth was 100 cm.

Model II

The Noah parameters of the loam soil type were directly applied or translated to establish an Expert-N model soil to mimic the soil properties of Model I. For this purpose, a 200-cm-deep soil profile comprising 40 numerical layers with identical soil properties was supposed. The rooting depth was set to 100 cm as in Model I. The soil texture was obtained from the State Soil Geographic Database (STATSGO) (Miller and White, 1998). Because of difficulties in transferring all the parameters, hydraulic properties were estimated using the Rosetta software (Schaap et al., 2001). Organic matter, rock fraction, and pH values were taken from Roth (2006). Soil properties were applied as presented in Table 1. Grassland growth was simulated using the Hurley Pasture Model (HPM) including harvest management.

Models III to V

Expert-N was applied using the site-specific soil description by Roth (2006) comprising a soil profile depth of 130 cm and five

Table 2. Measurement devices at the site station in Chamau.

Measurement	Instrument	Height
		m
Wind (three-dimensional sonic anemometer)	Solent R3, Gill Instruments	2.41
H_2O (open path infrared gas analyzer)	IRGA, Li-7500, Li-Cor	2.41
Air temperature and relative humidity	HydroClip S3, Rotronic	2
Photosynthetic photon flux density	K&Z PARlite, Kipp & Zonen	2
Short- and longwave radiation	CNR1 ventilated CNR1, Kipp & Zonen	2
Soil humidity	ML2x, Delta-T Devices	−0.5

horizons with 26 equidistant numerical layers and different soil basic parameters. Hydraulic properties were estimated using the Rosetta software (Table 1). Grassland growth was simulated using the HPM adapted to the Expert-N framework. Using this basic setup, the model was executed with three configurations to test the impacts of site-specific harvest management and different rooting depths on the simulated energy fluxes.

Model III. The rooting depth was limited to 130 cm. Harvest management was inactive.

Model IV. Harvest management was active, and the rooting depth was limited to 30 cm.

Model V. Harvest management was active, and the rooting depth was limited to 130 cm.

An overview of Models I to V is presented in Table 3. The individual submodel choices of Models II to V are provided in Table 4.

Model I accounts for vegetation growth dynamics using monthly mean values of the measured LAI on the 15th day of each month with linear interpolations. The monthly mean LAI values were applied on measurements presented by Gilgen and Buchmann (2009). In Models II to V, the HPM was applied using the parameter values of the original model as documented by Thornley (1998). Minor parameter adjustments were required to account for the site-specific species composition and to simulate realistic vegetation growth (see Table 5). The changes were made either using measured data or by adjusting these parameters by comparison with measured biomass data. All models were applied without further calibration.

Energy Flux Model Descriptions

Here, we present the general model concepts. More detailed model descriptions can be found in Appendix A and the associated literature. The submodel choices of Expert-N 5.0 are shown in Table 4.

All five models used the energy conservation equation to describe the energy fluxes at the surface layer:

$$R_n - H_s - L - G = 0 \quad [1]$$

where R_n is net radiation flux, H_s is sensible heat flux, L is latent heat flux, and G is ground heat flux.

Net Radiation Flux

Net radiation flux (R_n) is the net amount of radiant energy available at the vegetation surface. Thus, it is the difference between the net shortwave radiation and net longwave radiation. The net shortwave radiation is the non-reflected part of the shortwave radiation and can be calculated from the incoming shortwave radiation and the albedo (α). In Model I, α was derived using measured values. In Models II to V, α was estimated from the LAI ($m^2\ m^{-2}$) dynamics computed by the plant growth submodel HPM (see above) and from the albedo of the uncovered soil, which was calculated using the soil properties and the volumetric soil water content of the upper soil layer. Longwave radiation was calculated according to the Stefan–Boltzmann law in all five models. For more details, see Eq. [A1–A3].

Sensible Heat Flux

Model I used bulk transfer relationships (Garratt, 1993) for the calculation of H_s (Eq. [A25]). In Models II to V, H_s was calculated using a Penman-like approach. The residual energy of potential and actual latent heat was added to the sensible heat to close the energy balance and to take plant and soil water stress into account (Eq. [A14]).

Latent Heat Flux

In Model I, L was computed as the sum of soil evaporation, evaporation of the intercepted precipitation, and transpiration through the stomata (Eq. [A20–A23]). In Models II to V, L (Eq. [A5]) was computed from the potential evapotranspiration using a Penman–Monteith approach (Monteith, 1965, 1981). The potential evapotranspiration was then reduced depending on the water content in plants and soil, stomatal conductance (Eq. [A18]), and LAI (Eq. [A16]).

Ground Heat Flux

In Model I, G (Eq. [A24]) was calculated using the temperature gradient between the surface temperature and the midpoint

Table 3. Summary of the main differences among the five land-surface model approaches.

Model	Numerical layers	Horizons	Rooting depth	Profile depth	Harvest management
			cm		
I	4	1	100	200	no†
II	40	1	100	200	yes
III	26	5	130	130	no
IV	26	5	30	130	yes
V	26	5	130	130	yes

† Monthly interpolated measured LAI values

Table 4. Submodel configuration of Expert-N 5.0.

Submodel name	Operation	Reference
DAYCENT	soil: C, N turnover	Parton et al. (1998)
ADE LEACHN	soil: N transport	Hutson and Wagenet (1992)
HYDRUS	soil: water transport	Šimůnek et al. (1998)
van Genuchten & Mualem	hydraulic functions	van Genuchten (1980), Mualem (1976)
Daisy heat transfer	soil: heat flux	Hansen et al. (1991)
Hurley Pasture Model	aboveground plant growth	Thornley and Cannell (1997), Thornley (2001, 1998)
Feddes root model	root water transport	Feddes et al. (2001)

Table 5. Adjusted parameters in the Hurley Pasture Model. The 324 remaining plant model parameters were applied as presented by Thornley (2001, 1998).

Parameter	Value	Reference
Maximum stomatal conductance, m s^{-1} m^{-2} leaf	0.010 (0.005)†	Schulze (1994), Kelliher et al. (1995), Monteith (1993)
Proportional factor of leaf area index to canopy height, m m^{-2} leaf m^{-2} ground	0.15 (0.026)	measured‡
Conversion yield factor for structural plant growth	0.78 (0.75)	Amthor (2000)
Lamina partition factor	0.83 (0.7)	Robson (1973)
Michaelis–Menten constant for N uptake, kg N m^{-2}	0.002 (0.003)	Alt (2000), Peuke et al. (1996)
N uptake inhibition parameter, kg N kg^{-1}	0.01 (0.005)	Thornley (1998)

† Original values of Thornley (2001, 1998) in parentheses.
‡ Adjusted to match C and N concentrations in soil and plant substrates.

temperature of the first soil layer multiplied by the thermal conductivity. In Models II to V, G (Eq. [A4]) was calculated using the formulation of Choudhury (1989), which assumes that G depends on R_n and the LAI. The proportionality factor used in this formula differs between day and night.

Plant Growth

In Models II to V, vegetation dynamics, such as growth, C and N cycles, and water flow in the plant, were simulated using the HPM (Eq. [A16–A18]) (Thornley and Cannell, 1997; Thornley, 2001, 1998). The HPM assumes proportionality between the canopy height and the LAI ($h_{can} \propto$ LAI). The root water uptake was computed using the Feddes model (Feddes et al., 2001). The root biomass distribution declined exponentially with the rooting depth in the soil profile. The rooting depth of the simulated grasslands was assumed to be constant throughout the simulation period. In contrast to Models II to IV, Model I neglected mechanistic plant growth dynamics. In this case, to compute the net radiation flux, the canopy was represented by LAI dynamics with linear interpolation between the measured monthly mean values following Pan and Mahrt (1987).

Soil Water

Model I described the soil profile by four numerical layers with identical soil properties for each layer (Mahrt and Pan, 1984; Schaake et al., 1996). The soil water transport was computed using the diffusivity form of the Richards equation. The diffusivity form was defined by the formulation of Cosby et al. (1984) for nine different soil types (see also Appendix A2). Models II to V computed the water transport using the HYDRUS submodel, i.e., the mixed form of the Richards equation, to account for the hydraulic properties of the soil horizons (Šimůnek et al., 1998).

Data Analysis

The performance of the different model approaches was tested by comparing the simulated energy fluxes (L, H_s, and R_n) with the hourly mean flux tower measurements using the Nash–Sutcliffe efficiency (NSE) and the root mean square error (RMSE). The NSE was defined as

$$\mathrm{NSE} = 1 - \frac{\sum_{i=1}^{N}(P_i - O_i)^2}{\sum_{i=1}^{N}(O_i - \bar{O})^2} \quad [2]$$

where P_i is the prediction, O_i is the observation, and $\bar{O}$ is the mean of the observations. The NSE can range from $-\infty$ to 1. If NSE = 1, the predicted data perfectly match the observed data. An NSE > 0 indicates that the predicted values better represent the observations than the mean of the observed values (Nash and Sutcliffe, 1970).

The RMSE was computed as

$$\mathrm{RMSE} = \sqrt{N^{-1}\sum_{i=1}^{N}(P_i - O_i)^2} \quad [3]$$

Results

The simulation results were compared with flux tower measurements of an intensively managed grassland site in Switzerland in 2006 and were evaluated for three different periods: (i) the main vegetation growth period (May–September); (ii) a period in May during which the measured water-filled pore space (WFPS) at a depth of 5 cm exceeded 0.80; and (iii) a period in July during which the driest soil conditions at a depth of 5 cm were observed and WFPS ranged between 0.40 and 0.60.

Plant Growth Simulations

Models II to V simulated daily average aboveground biomass growth rates of 4 to 7 g m^{-2} d^{-1} from May to August 2006, with maximum rates of 20 g m^{-2} d^{-1} and minimum values of 0.1 g m^{-2} d^{-1}. Because Model I does not simulate dynamic plant growth, no growth rates were calculated.

Statistical evaluations (RMSE) indicated that the ability of the models to simulate the measured LAI dynamics declined in the order: I > IV > II > V > III. Model III, the model with the highest RMSE (1.1 m^2 m^{-2}), underestimated the LAI in June but overestimated it twofold in July, reaching LAI values of >7 m^2 m^{-2} at the end of August. Such high LAI values together with canopy heights

of up to 1.2 m are realistic for extensively managed hay fields at low alpine altitudes (Körner, 2003). Under the intensively managed conditions of the pasture examined in the present study, the measured late-season values are overestimated almost threefold. In the simulations by Models II, IV, and V, the LAI values declined to 0.5 after harvest events due to the model assumption by Thornley (1998) that the LAI is proportional to the canopy height, which declined due to cutting. The measured LAI values were underestimated by 20 to 55%. In agreement with the measurements, a maximum LAI of approximately 2.5 m^2 m^{-2} was simulated in mid-July before the third harvest event. Based on its RMSE value (0.31 m^2 m^{-2}), Model I best simulated the LAI dynamics via linear interpolations between monthly mean measurements. However, Model I failed to capture the abrupt declines of LAI at harvest followed by the increase in LAI due to canopy regrowth (Fig. 1).

Soil Water Storage Simulations

Model I simulated well to the 5-cm soil depth the dynamics of the two drier periods, which were separated by a short rewetting event (Fig. 2). However, the simulations strongly underestimated the WFPS by approximately 25% during the more moist periods from May to mid-June and in August. Consequently, lower amplitudes of WFPS dynamics were simulated, ranging from maximum values of <0.70 to minimum values >0.45.

In the simulations by Model II, the near-surface soil moisture in the 5-cm soil depth was mostly near saturation (WFPS > 0.75) (Fig. 2). Only during two drier periods in mid-June and at the end of July did the WFPS decline to values between 0.60 and 0.55. During both periods, the WFPS was mostly overestimated, particularly after the short mid-June drought period and during the rewetting phase (Fig. 2) at the beginning of August, when the measured WFPS was mostly <0.5 but the simulated values were >0.90.

On average, Model IV underestimated the WFPS measurements by 0.05. The largest underestimations occurred with the onset of topsoil drying in June and peaked in late July with WFPS values of <0.20 when the measurements were still >0.40. This underestimation was due to the shallow rooting depth of 30 cm, which was assumed following the documentation by Roth (2006). In the simulations, this limitation of rooting depth caused stronger topsoil drying because water resources from deeper soil layers were not available to fulfill the transpiration demands of the vegetation. After rewetting at the end of August, the WFPS in the upper 5 cm matched the measured dynamics.

The WFPS simulations by Models V and III underestimated the measured values until mid-June due to the possibly too deep rooting depth assumptions in the models. Both models surprisingly overestimated by 0.20 the WFPS in the topsoil during the rewetting event. This overestimation might be due to lateral runoff in the field, which was not considered in the simulations. Model V captured the soil drought peak in late July (WFPS = 0.42), while the simulations by the model without biomass harvest (Model III) obtained a higher topsoil moisture of 0.50. The lower topsoil moisture obtained by Model V (compared with Model III) was due to a decrease in the simulated LAI to 0.5 m^2 m^{-2} by harvest, which abruptly increased the evaporation rates from bare soil and consequently dried the topsoil, which did not occur using Model III. Without harvest, the simulated LAI values exceeded 4.0 m^2 m^{-2} and prevented any evaporation. Water was thus extracted by deep roots (130 cm) and the topsoil remained more moist (WFPS = 0.50) due to the prevention of evaporation. Strong topsoil drying was observed in simulations by Model II after harvest when the LAI values were small because of the rapid dehydration of the soil profile, which in this case was assumed to be homogeneous.

Dynamic of the Energy Fluxes

Energy fluxes related to the land-surface layer comprise the ground heat flux, G, the latent heat flux, L, which is proportional to the sum of transpiration and evaporation (Fig. 3), the sensible heat flux, H_s (Fig. 4), and the net radiation, R_n. We analyzed the ability of the five different models to simulate the dynamics of the sensible and latent heat fluxes. The net radiation fluxes were well described by all models (Models II–V [NSE > 0.94] and Model I [NSE = 0.85]), and no deeper analysis or discussion is needed. The net radiation flux simulations and corresponding measurements including the ground heat fluxes are provided below in the Supplemental Material.

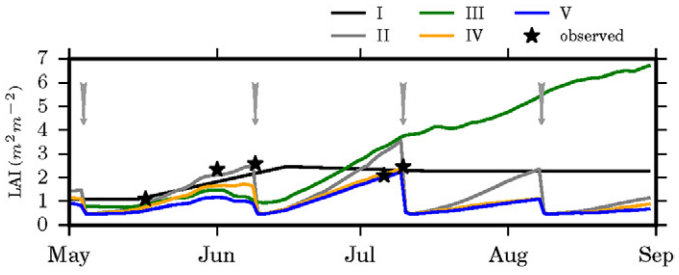

Fig. 1. Measured (asterisks) and simulated (solid lines) dynamics of the leaf area index (LAI) from 1 Mar. to 1 Sept. 2006 using Models I (black), II (gray), III (green), IV (orange), and V (blue). Vertical arrows are biomass harvest events.

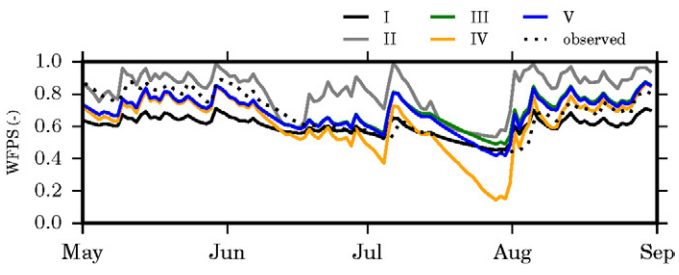

Fig. 2. Measured (dotted line) and simulated (solid lines) dynamics of the water-filled pore space (WFPS) at a soil depth of 0.05 m from 1 Mar. to 1 Sept. 2006 using Models I (black), II (gray), III (green), IV (orange), and V (blue).

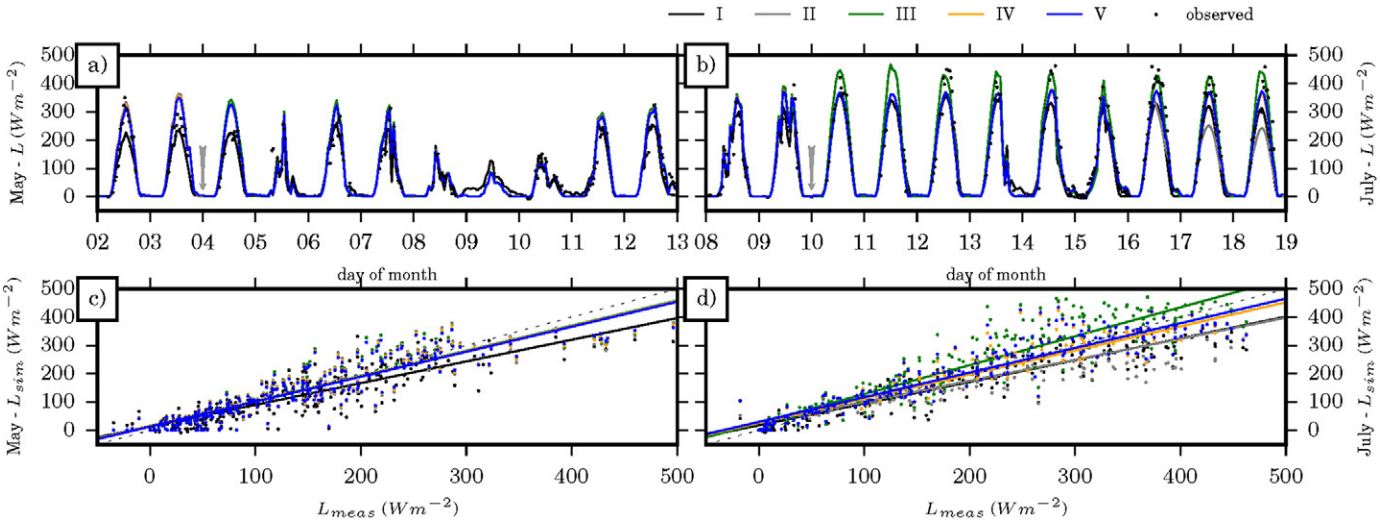

Fig. 3. Measured (dots) and simulated (solid lines) dynamics of latent heat flux (L) from (a) 2 to 13 May (temperate, moist) and (b) 8 to 19 July (hot, dry), and (c,d) measured vs. simulated values using Models I (black), II (gray), III (green), IV (orange), and V (blue). Vertical arrows are biomass harvest events.

Latent Heat

In May (moist and temperate), four models (II–V) overestimated the measured values by approximately 110 W m^{-2} on the day after harvest (Fig. 3). Model I simulated the latent heat flux dynamics very well after harvest but underestimated the daily peak values before harvest by 50%. The harvest (Models II, IV, and V) had no significant impact on the latent heat flux simulations. Figure 3c shows that energies between 110 and 130 W m^{-2} were, on average, well simulated by all examined models. All models tended to underestimate higher energies and overestimate lower energies. This pattern was most evident in simulations by Model I. Only small differences among the simulations of Models II to V in May (no water stress) were observed, and the simulated LAI values were low, approximately 1.0 m^2 m^{-2}. The consequence was that the latent heat flux depended largely on the evaporated soil water.

Around the beginning of July, the latent heat flux simulations by Models II to V did not differ significantly. After harvest, the latent heat flux simulations of Model III exceeded the simulation results of all other models by up to 150 W m^{-2} (Fig. 3b and 3d) due to the simulation of excessively high LAI values (Fig. 1). Until 4 d after harvest, the latent heat flux simulations did not differ significantly among Models I, II, IV, and V. On 17 July, the simulation results of all models varied strongly, particularly when the fluxes exceeded 200 W m^{-2} (Fig. 3b). Among all five models, the fluxes were simulated with declining highest daily peak values in the order II > I > IV > V > III. The main reason for this apparent delay was the different levels of water stress (amounts of plant-available water) experienced by the vegetation in the five different simulations. The daily mean fluxes exhibited an identical trend (Fig. 5). The simulated differences in latent heat fluxes among the models continued

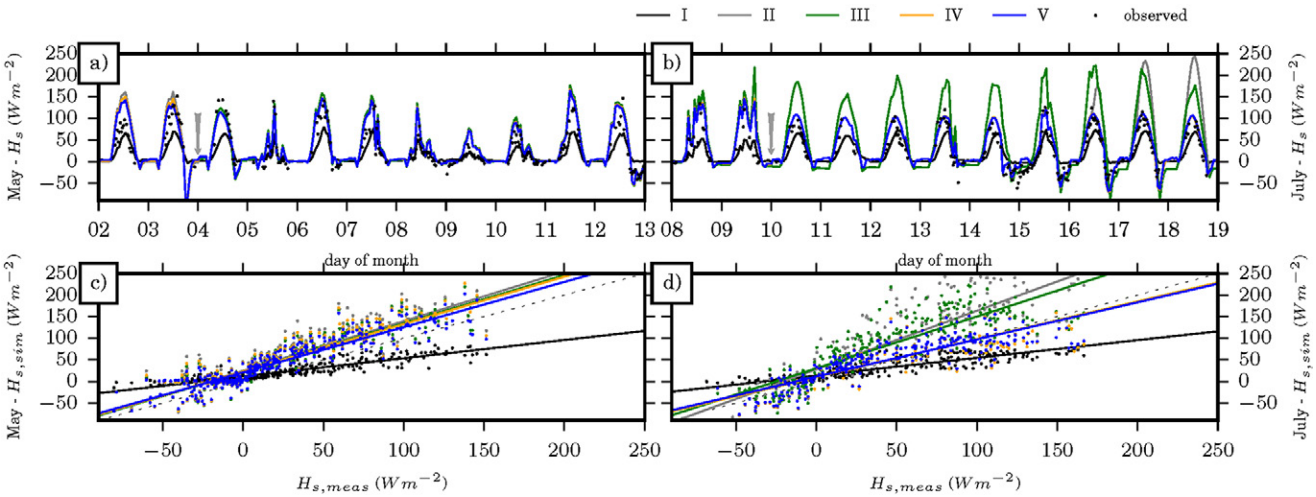

Fig. 4. Measured (dots) and simulated (solid lines) dynamics of sensible heat flux (H_s) from (a) 2 to 13 May (temperate, moist) and (b) 8 to 19 July (hot, dry), and (c,d) measured vs. simulated values using Models I (black), II (gray), III (green), IV (orange), and V (blue). Vertical arrows are biomass harvest events.

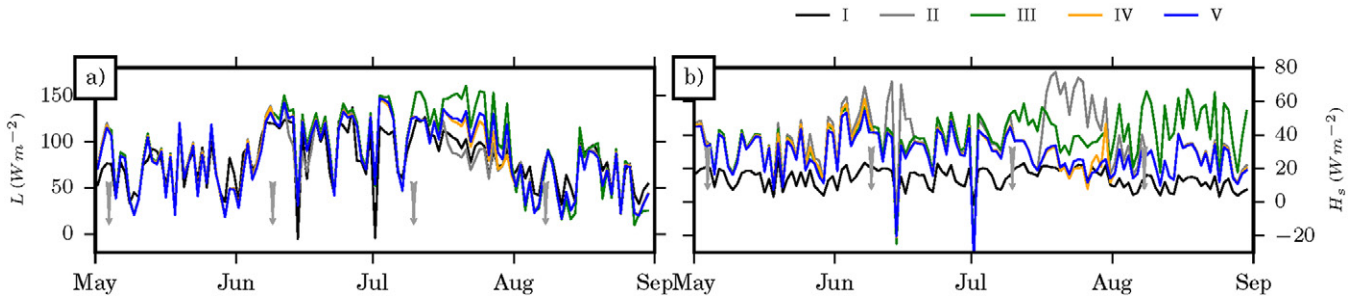

Fig. 5. Simulated (solid lines) daily dynamics of (a) latent heat flux (L) and (b) sensible heat flux (H_s) from 1 Mar. to 1 Sept. 2006 using Models I (black), II (gray), III (green), IV (orange), and V (blue). Vertical arrows are biomass harvest events.

until soil rewetting in August. The strongest underestimations of high energies were observed in simulations by Model I.

Sensible Heat

In May (moist and temperate), no significant differences among the simulations of Models II to V (harvest management, rooting depth, and different descriptions of soil properties) were observed (Fig. 4a). These models systematically overestimated the sensible heat by between 10 and 30 W m^{-2} for small energies (<0 W m^{-2}) and high energies (>100 W m^{-2}), respectively. The fitted mean line was nearly parallel to the bisector of the first quadrant (Fig. 4c). The amplitudes in sensible heat flux simulations by Model I were lower than those in the simulations by all other models (Fig. 4a) in May, July (Fig. 4b), and throughout the simulation period (Fig. 5b).

Model I underestimated the fluxes above 100 W m^{-2} by up to 50% and also overestimated the negative fluxes by up to 50% at 25 W m^{-2} (Fig. 4c). Energies between 25 and 0 W m^{-2} exhibited small deviations between the simulations and measurements.

In July (dry and hot) before the harvest event, no significant differences among the sensible heat flux simulations of Models II to V were observed (Fig. 4b). After the harvest, Model III (the model without harvest management) simulated between 50 and 100% higher fluxes than the models that included harvest management for a period of 6 d (Model II; Fig. 4b) and until the end of the simulation period compared with simulations by Models IV and V. The increasing bias of latent heat flux simulations by Model III compared with the simulations by Models IV and V after the subsequent harvest event in August was significant. Moreover, due to the assumption of proportionality in LAI and canopy height in the HPM submodel, a higher LAI increased the surface roughness length, which decreased the aerodynamic resistance, generating turbulence and consequently higher H_s (Park et al., 2011).

Our simulation results and the underlying model assumptions emphasize the strong impact of abrupt changes in canopy height and leaf area in harvest-managed grassland ecosystems during drought periods. The strong soil drying of the soil profile with homogeneous soil properties in simulations by Model II after harvest in July resulted in an abrupt increase in sensible heat fluxes, reaching daily average values of 80 W m^{-2} (Fig. 5b). This abrupt increase occurred due to rapid soil drying of the homogeneous soil profile after harvest and consequently limited plant-available water for transpiration. Throughout the growing season, the lowest daily mean (<25 W m^{-2}) sensible heat fluxes (during the day) were simulated by Model I.

The sensible heat flux dynamics did not respond to water stress because in Model I, the sensible heat fluxes were computed as the residuum from the energy balance (Eq. [1]) after the elimination of R_n, L, and G. The lower simulated latent heat fluxes (up to 50% compared with simulations by Models II to V, Fig. 4a and 4b) were compensated by the higher ground heat fluxes (up to 60%).

The maximum differences observed among the simulated dynamics of the net radiation fluxes of the five models were <50 W m^{-2}, which was <7% of the net radiation flux. Figure 4c and 4d demonstrate the small response of the sensible heat flux simulations by Model I. However, overestimations of the sensible heat fluxes were observed in the simulations by Models II and III. The sensible heat flux simulations by Models IV and V had high accuracy (NSE $\approx$ 0.65). We conclude that Model I did not respond to the limited soil water availability in the permanent grassland simulations. The most accurate water stress responses were simulated by Models IV and V, for which the measured and simulated H_s values in July nearly matched the 1:1 line (Fig. 4d). High energies were often overestimated by Models III and II and underestimated by Model I.

Statistical Analysis

Figure 6 shows the NSE of the energy balance simulations for different time ranges. Latent heat flux dynamics simulations revealed NSEs between 0.8 (Models V and IV) and 0.7 (Model I) between May and August. Overall, averaging the NSE values of R_n, L, and H_s shows that $NSE_{average}$ of each model was >0.4 (Fig. 6c). The largest variations among the models between May and August were observed for sensible heat flux dynamics: the NSEs were 0.6 for Model V and 0.5 for Models IV and I, but 0.1 and −0.4 for the simulations by Models II and III, respectively.

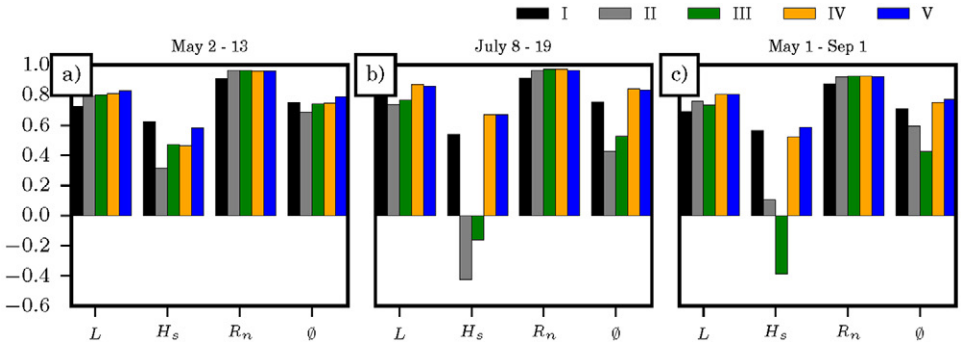

Fig. 6. Nash–Sutcliffe Efficiencies (NSE, vertical bars) for the simulations of latent heat (L), sensible heat (H_s), and net radiation (R_n) fluxes and the averaged NSE (∅) for (a) 2 to 13 May, (b) 8 to 19 July, and (c) 1 May to 1 September 1 using Models I (black), II (gray), III (green), IV (orange), and V (blue).

At the beginning of the vegetation period in May, when the weather conditions were moist, Models III and II performed better at simulating the dynamics of the measured energy fluxes (latent heat: NSE ≈ 0.8; sensible heat: NSE > 0.25). In July, their average performances decreased to approximately 0.5 (latent heat: NSE ≈ 0.8; sensible heat: NSE < 0.0). Models II and III could not accurately represent the sensible heat because the ground heat flux was five times lower than that of the other models due to an unrealistically high LAI (Model III) or an overly simplistic description of the soil properties causing topsoil drought (Model II).

Models V, IV, and I produced similar results in May and July. Dryness did not affect the performance of these models (latent heat: NSE ≈ 0.8; sensible heat: NSE > 0.4). In particular, the sensible heat flux appears to be very sensitive to soil properties and harvest management, which is correlated to the LAI.

Figure 6c presents the time range from May to September. Overall, all models produced an almost identical NSE for the net radiation (≈0.9). The latent heat was best represented by Models V and IV (≈0.8). The other NSE values ranged between 0.8 and 0.6. The sensible heat was the most sensitive variable in the models: whereas the performance of Models V, IV, and I was stable, with values between 0.45 and 0.50, Models III (the model with no harvest) and II (the model with homogeneous soil properties) had low NSE values (Model III: −0.4; Model II: 0.1). In summary, the simulations by the models without harvest and with a simplified representation of the soil properties had difficulty reproducing the measured values. Comparing the average NSE values (latent heat, sensible heat, and net radiation) leads to the conclusion that Models V and IV best simulated the measured values, closely followed by Model I. Models III and II did not satisfactorily simulate the fluxes, particularly in view of the complexity of these models.

The RMSE results are shown in Fig. 7. Across the complete time range (May–September), the RMSE averages are between 48 and 59 W m^{-2}. Comparing the RMSEs of latent heat, sensible heat, and net radiation leads to the conclusion that Models V and IV best simulated the measured values. Models I, II, and III did not perform as well and had almost similar results.

Discussion

Plant Growth

The simulated growth rate is a good indicator to evaluate overall model performance. This was only possible using Models II to V based on Expert-N. The simulated maximum growth rates were about 38% lower than those simulated by Hurtado-Uria et al. (2012) using a stand-alone model version of the HPM to simulate 27 yr of permanent grassland growth in Ireland. They observed daily average values between 3 and 32 g m^{-2} d^{-1} but also systematically overestimated the measured values, particularly during summer drought. Such overestimations of growth rates were not observed in our simulations, in part due to the more detailed description of the soil water flow using the HYDRUS model and the Feddes root water uptake model (see Table 4) as well as due to the different parameterization of plant growth (Table 5). This is in contrast to the soil water flow model originally applied in the HPM, which uses a simple bucket approach based on only one numerical soil layer. Therefore the original HPM often fails to simulate dry conditions at the soil surface and hence plant water stress

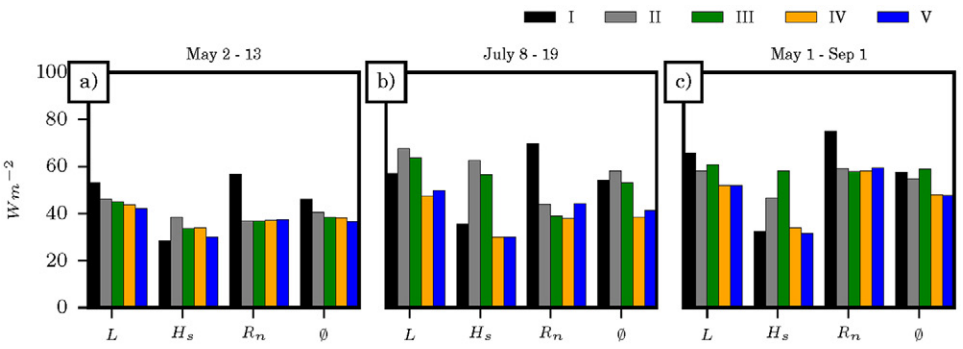

Fig. 7. Root mean square errors (RMSE, vertical bars) for the simulations of latent heat (L), sensible heat (H_s), and net radiation (R_n) fluxes and the averaged RMSE (∅) for (a) 2 to 13 May, (b) 8 to 19 July, and (c) 1 May to 1 September using Models I (black), II (gray), III (green), IV (orange), and V (blue).

at the topsoil. The accuracy of the five models in simulating plant growth and LAI dynamics was evaluated. In May, Hurtado-Uria et al. (2012) observed growth rates between 6 and 12 g m^{-2} d^{-1}. In our simulations, we observed growth rates between 3.7 and 5.3 g m^{-2} d^{-1}. These differences are probably due to differences in the weather conditions, the soil properties, the site management, and the species compositions between Switzerland and Ireland. The observed declines in growth rates were simulated by Model III, in which the growth rates declined from 9 to 3 g m^{-2} d^{-1} in July in response to summer drought. No drought depression was observed in the simulations by Model II, and the growth rates even increased from 6 to 8 g m^{-2} d^{-1}.

All the models reacted to drought events, and it is known that drought can elicit changes in grassland dynamics through a variety of other mechanisms (Thomas et al., 1989). Most of these mechanisms are not yet considered in our models, but they could be potentially important to understand the disparity of responses observed in field studies. The responses can be physical, which was shown by Thomas et al. (1989) and Chaves (2002). Some species can also resist or avoid water stress through enhanced water uptake at low soil water potentials (Volaire and Lelièvre, 2001; Volaire, 2008). This leads in the long term to shifts related to the composition of the grassland community (e.g., Gilgen et al., 2010; Mariotte et al., 2013), which cannot be represented by the considered Models I to V.

However, based on the evaluation of the LAI and the energy fluxes, we determined that Models IV and V simulated the energy fluxes with high accuracy because they were able to reflect the changes in the LAI. Compared with the other models, Model I uses interpolated LAI values based on measured data as input, which resulted in a lower NSE. The description of the LAI dynamics of Model III, which ignored harvest management, failed to adequately simulate the sensible and ground heat fluxes during drought periods.

We conclude, similar to Tsarouchi et al. (2014), that the implementation of dynamic crop development leads to more accurate evapotranspiration simulations if the management is correctly represented. The impact of harvest was in particular high during the dry period. In the study of Tsarouchi et al. (2014), the static LAI model overestimated measured values during the dry period, in contrast to our simulation, where the simulated values were mostly underestimated by Model I due to the lack of a dynamic LAI simulation.

Harvest Management and Soil Properties

The models without harvest (Models I and III) or with a simplistic description of soil properties (Models I and II) had no problems simulating the latent and sensible heat fluxes during the wet months but could not accurately represent the sensible heat and ground heat flux during the dry months. Too high LAIs (Model III) and an overly simplistic description of the soil properties caused topsoil drought (Model II). In fact, that the harvest frequency is very important when simulating managed grassland was also shown by Ammann et al. (2007). They found that the cutting frequency has a strong impact on the C dynamics and on energy fluxes. Mahmood and Hubbard (2003) also came to the conclusion that harvest management can be very important and that especially plant growth dynamics determines the surface energy exchange dynamics. If harvesting was completely neglected (Model III), the LAI rose to unrealistic values. The higher LAI in the simulations by Model III resulted in much higher ground cover, and consequently, the ground heat flux energy was reduced to one-fourth that of simulations by Models II, IV, and V. The other possibility to avoid a harvest model was to use measured and/or averaged monthly values (Model II). The results were much better and the energy fluxes were acceptable. The model had problems, especially after cutting or subsequent to extreme events like drought, because even if the average of the LAI was correct, the dynamic of the LAI was very important, especially during dry periods. This was also the conclusion of Tsarouchi et al. (2014). Lin and Cheng (2016) showed that latent and sensible heat simulations are very sensitive to soil texture and moisture initialization, and Mahmood and Hubbard (2003) came to the conclusion that soils with higher water capacities buffer the crop physiology against stress. In wet years, these effects were smaller. These results are similar to our findings. Mahmood and Hubbard (2003) assumed that the effects of different soil descriptions are less important than those of the land use and management.

Our results showed that in a homogeneous soil the differences in surface energy fluxes compared with models with a more detailed soil description (Models I and II) were negligibly small. Only droughts had a huge impact; the sensible heat flux especially was very sensitive. We conclude that the sensible heat was strongly influenced by the rooting depth and the soil parameterization when the soil was dry. The models with higher complexity of soil descriptions (Models IV and V) were much more stable under drought and abrupt water content changes in the soils.

Rooting Depth

To understand the impact of the rooting depth, two models with different rooting depths were analyzed. One model (IV) was configured to the shallow rooting depth of 30 cm, following the site documentations of Roth (2006). The other model (V) considered rooting throughout the entire soil profile (130 cm). Our results show that limitation of the rooting depth to 30 cm caused stronger topsoil drying and in consequence low NSE values because water resources from deeper soil layers were not available to satisfy the transpiration demands of the vegetation. We conclude that at least some of the grassland species rooted in deeper soil layers. Deeper rooting is very likely because this grassland comprises approximately 25 species (Gilgen and Buchmann, 2009). Dierschke and Briemle (2002) and Herndl et al. (2011) observed that most grass species root in the upper soil layers and

rarely root deeper than 30 cm. By contrast, Brown et al. (2010) demonstrated that 20 out of 41 grass species root deeper than 70 cm, with 5 to 15% of the total root biomass deeper than 68 cm. However, the observations of Brown et al. (2010) might be biased by a pot effect in that specific experiment. Gilgen et al. (2010) described a weed problem with *Rumex obtusifolius* L. at this site and a high diversity of the grassland community. *Rumex* and other herbs such as *Plantago lanceolata* L. may easily root in deeper soil layers. Gayler et al. (2014) showed for field crops that it is possible to improve a model with dynamic root growth and concluded that the root biomass and rooting depths change considerably throughout the vegetation period. In contrast to field crops, the rooting depth of permanent grasslands does not change much throughout the year (Sindhøj et al., 2000; Fiala, 2010), but a dynamic root growth model could react to different environmental triggers with either enhanced root growth or death, especially under drought (Monteith, 1991). This could reduce the sensitivity of grassland ecosystem simulations to persistent water stress. This complexity is not fully understood and is discussed controversially. Some responses, e.g., to drought, were analyzed and found in arid environments (Kalapos et al., 1996; van Wijk, 2010) but could not be found in other experiments (Walter et al., 2012; Prechsl et al., 2014).

Based on our simulations, we conclude that, especially during droughts, it could be an advantage to allow rooting through all horizons. A dynamic root growth model could improve the simulations as it is able to respond to drought or nutrient shortages.

Summary and Conclusions

In this study, we analyzed the ability of five different models to simulate measured energy fluxes in the plant–soil–atmosphere system subject to management. These models included four different Expert-N 5.0 model configurations and the widely applied LSM Noah.

The five model approaches differed in the complexity of their descriptions of the site-specific physical soil properties, the different maximum rooting depths, and the consideration of biomass growth and harvests. The models were evaluated against data for grassland growth and corresponding flux-tower measurements at Chamau, Switzerland, in the year 2006.

We conclude that the abrupt decline of LAI at harvest followed by LAI regeneration due to plant growth cannot be neglected in energy flux simulations. In addition, dynamic vegetation models including root growth and more detailed, site-specific descriptions of physical soil properties can improve simulations of energy fluxes from the land surface to the atmosphere. The degree of improvement, however, depends on the season, the complexity of the soil profile, and the land-use management. During summer, when high temperatures cause drought, the rooting depth may have a strong impact on how much water is extracted from the soil profile and, in particular, from the relevant near-surface soil layers. This influence of the rooting depth in summer strongly affects transpiration and evaporation (when the LAI values are small) and consequently, strongly impacts the energy flux simulation results.

The performance of more complex models usually increases with the amount of information that is available on the ecosystem of interest, and it is challenging to improve the availability of such data, in particular, because complete ecosystem descriptions at high spatial resolution are rare. In the absence of information, ad hoc assumptions may be helpful, but good descriptions of ecosystem heterogeneity and management timing in a region are needed to significantly improve energy flux simulations between the land surface and the atmosphere. This then could also improve weather forecasts at the regional scale.

Appendix A: Model Descriptions

Here we give an overview of the governing model equations that were applied to simulate surface energy fluxes, plant growth, and soil water transport. Model I is the original Noah model. The only change was the use of adjusted LAI values to simulate realistic site-specific LAI dynamics (Appendix A2). Models II to V are all applications of the model system Expert-N (Appendix A1). In these four models, the soils are described using different levels of detail (site-specific or more general). Plant growth is described using the HPM model using the same parameterization in all models. The differences in observed plant growth dynamics are due to different rooting depth constraints and whether harvest management is considered or not.

Appendix A1: Expert-N 5.0

The model system Expert-N 5.0 comprises mechanistic ecosystem submodels to simulate matter, water, and energy fluxes in the soil–plant–atmosphere system. The system consists of various submodels for the water cycle, heat transfer, plant growth, and the N cycle. The description presented here refers to the respective submodel choices shown in Table 4, which were used for the simulations in this study. The mathematical description could be different for other submodule choices.

Surface Energy

In the energy balance, R_n is the net amount of radiant energy available at the vegetation surface and is given by

$$R_n = R_{ns} - R_{nl} \quad [A1]$$

as the difference between the net shortwave radiation, R_{ns} (W m^{-2}), and net longwave radiation, R_{nl} (W m^{-2}). The non-reflected part of the incoming solar radiation, R_{ns} (W m^{-2}), is determined by

$$R_{ns} = R_s - \alpha R_s \quad [A2]$$

The reflected part is described as αR_s, where α (dimensionless) is the albedo, which depends on the leaf area index, LAI ($m^2\ m^{-2}$), and the volumetric water content of the upper soil layer, $\theta_{soil,1}$ (dimensionless). The value of R_{nl} is calculated according to the Stefan–Boltzmann law, which was introduced by Brunt (1932, [1954] 2011) as

$$R_{nl} = \sigma f_{cd}\left(0.34 - 0.14\sqrt{e_a}\right)T_K^4 \quad [A3]$$

where σ ($W\ K^{-4}\ m^{-2}$) is the Stefan–Boltzmann constant, f_{cd} (dimensionless) is the calculated cloudiness factor, e_a (kPa) is the actual vapor pressure, and T_K (K) is the surface air temperature.

The value of G ($W\ m^{-2}$) is assumed to be proportional to R_n for constant LAI values (Choudhury, 1989; Choudhury et al., 1987). The proportionality factor differs between day and night. Hence G is given by

$$G = \begin{cases} 0.4\exp(-0.5\mathrm{LAI})R_n & \text{for daytime} \\ 2.0\exp(-0.5\mathrm{LAI})R_n & \text{for nighttime} \end{cases} \quad [A4]$$

and L is given by

$$L = \frac{10^6}{3600}\rho_w L_{evap}\mathrm{ET}_{act} \quad [A5]$$

where L_{evap} ($MJ\ kg^{-1}$) is the latent heat factor (Allen, 2005; Allen et al., 2006), ρ_w ($Mg\ m^{-3}$) is the density of water, $10^6/3600$ ($h\ J\ s^{-1}\ MJ$) is a conversion factor, and ET_{act} ($mm\ h^{-1}$) is the actual evapotranspiration, that is, the sum of the actual evaporation, E_{act} ($mm\ h^{-1}$), and the actual transpiration, T_{act} ($mm\ h^{-1}$):

$$\mathrm{ET}_{act} = E_{act} + T_{act} \quad [A6]$$

The calculation of ET_{act} is based on the hourly potential evapotranspiration, ET_{pot} ($mm\ h^{-1}$), from Penman–Monteith (Monteith, 1965, 1981):

$$\mathrm{ET}_{pot} = 3600\frac{\Delta(R_n - G)10^{-6} + \rho_a c_p\left[(e_s - e_a)/r_a\right]}{\left[\Delta + \gamma\left(1 + r_s/r_a\right)\right]\rho_w L_{evap}} \quad [A7]$$

where Δ ($kPa\ K^{-1}$) is the slope of the saturation vapor pressure temperature curve, γ ($kPa\ K^{-1}$) is a psychometric constant, e_s (kPa) is the saturated vapor pressure, e_a (kPa) is the actual vapor pressure, and ρ_a ($kg\ m^{-3}$) and c_p ($MJ\ kg^{-1}\ K^{-1}$) are the mean air density and the specific heat of air, respectively. The factors 3600 ($s\ h^{-1}$) and 10^{-6} ($MJ\ J^{-1}$) are conversion factors, r_a ($s\ m^{-1}$) is the aerodynamic resistance, and r_s ($s\ m^{-1}$) is the surface resistance. Following Chenge and Brutsaert (2005) and Brutsaert (1982), r_a is calculated by

$$r_a = \frac{1}{k^2 u_z}(A_1 - B\Psi_m)(A_2 - B\Psi_h) \quad [A8]$$

with

$$A_1 = \ln\left(\frac{z_w - d_0}{z_{0m}}\right),\ A_2 = \ln\left(\frac{z_w - d_0}{z_{0h}}\right),\ \text{and}\ B = \frac{z_w - d_0}{L_{MO}}$$

where z_w (m) is the height of the wind measurements; d_0 (m) is the zero plane displacement height; z_{0h} (m) and z_{0m} (m) are the roughness lengths of heat and momentum, respectively; L_{MO} (m) is the Obukhov length; k (dimensionless) is the von Kármán constant; and u_z ($m\ s^{-1}$) is the wind speed. The stability functions Ψ_m and Ψ_h (both dimensionless) were described by Brutsaert (1982) and Chen et al. (1997). The plant surface resistance, r_s ($s\ m^{-1}$), is computed using the stomatal conductance, g_s ($m\ s^{-1}$), and the active (sunlit) leaf area index, LAI_{act} ($m^2\ m^{-2}$), which is assumed to be 0.5LAI:

$$r_s = \frac{1}{0.5\mathrm{LAI}\,g_s} \quad [A9]$$

The potential evaporation, E_{pot} ($mm\ h^{-1}$), is calculated as ET_{pot} reduced by the area of bare soil (not covered by plant biomass):

$$E_{pot} = \exp(-k_{can}\mathrm{LAI})\mathrm{ET}_{pot} \quad [A10]$$

where the plant cover fraction is given by $1 - \exp(-k_{can}\mathrm{LAI})$ following Raes et al. (1986), where k_{can} ($m^2\ m^{-2}$) is the leaf extinction coefficient. With the help of this plant cover fraction, the potential transpiration, T_{pot} ($mm\ h^{-1}$) can be derived:

$$T_{pot} = \mathrm{ET}_{pot} - E_{pot} \quad [A11]$$

For a given maximum amount of water that can be evaporated from the soil, $E_{pot,max}$ ($mm\ h^{-1}$), and maximum amount of water that can be transpired from the plant, W_{sh} ($mm\ h^{-1}$), the actual evaporation E_{act} and transpiration T_{act} can be calculated using

$$E_{act} = \min\left(E_{pot,max}, E_{pot}\right) \quad [A12]$$

$$T_{act} = \min\left(W_{sh}, T_{pot}\right) \quad [A13]$$

The shoot water content W_{sh} is a function of the relative shoot water content θ_{sh} of the plant (Thornley, 1998).

The sensible heat flux H_s is calculated as the residual component of the surface energy balance (Eq. [1]):

$$H_s = H_{s,pot} + \frac{10^6}{3600}\rho_w L_{evap}\left(\mathrm{ET}_{pot} - \mathrm{ET}_{act}\right) \quad [A14]$$

The potential sensible heat flux ($H_{s,pot}$) can be written in a similar form to ET_{pot} (Eq. [A7]):

$$H_{s,pot}=\frac{\gamma\left(1+r_s/r_a\right)\left(R_n-G\right)-3600\rho_a c_p\left[\left(e_s-e_a\right)/r_a\right]}{\Delta+\gamma\left(1+r_s/r_a\right)} \quad [A15]$$

Plant

Vegetation growth dynamics were simulated using the HPM (Thornley and Cannell, 1997; Thornley, 2001, 1998). The most important plant parameters related to the flux exchange model are the LAI ($m^2\ m^{-2}$) and the stomatal conductance, g_s ($m\ s^{-1}$). In the HPM, the LAI is divided into four age classes (Thornley, 1998). These LAI age classes sum to the LAI:

$$\mathrm{LAI}=\sum_{i=1}^{4}\mathrm{LAI}^i \quad [A16]$$

Each leaf area age class is calculated using an independent pool:

$$\frac{d\mathrm{LAI}^i}{dt}=I_{\mathrm{LAI}}^i+k_{\mathrm{turn}}\mathrm{LAI}^i-k_{\mathrm{deg}}\mathrm{LAI}^i-O_{\mathrm{LAI}}^i \quad [A17]$$

$$\text{with}\begin{cases}I_{\mathrm{LAI}}^{i=1}=\nu f_{\mathrm{lam}}G_{\mathrm{sh}}\\ I_{\mathrm{LAI}}^{i\neq1}=k_{\mathrm{turn}}\mathrm{LAI}^{i-1}\end{cases}$$

$$\text{and } O_{\mathrm{LAI}}^i=O_{\mathrm{LAI,an}}^i+O_{\mathrm{LAI,hv}}^i$$

Every equation of the pools (i) consists of four terms. The input rate I^i_{LAI} ($m^2\ m^{-2}\ d^{-1}$) is the leaf area input for each part. For $i = 1$, I^i_{LAI} is the product of the specific leaf area, ν ($m^2\ kg^{-1}$), f_{lam} (dimensionless) is the fraction of the leaf area, and G_{sh} ($kg\ m^{-2}\ d^{-1}$) is the actual growth rate of the shoot. For $i \neq 1$, I^i_{LAI} is the LAI flow from the younger leaf area age class ($i - 1$). The amount of flow is regulated by the turnover rate, k_{turn} (d^{-1}). The degeneration of the LAI is controlled by the degradation rate, k_{deg} (d^{-1}); the LAI is also decreased by animal grazing, $O^i_{\mathrm{LAI,an}}$ ($m^2\ m^{-2}\ d^{-1}$), and harvesting, $O^i_{\mathrm{LAI,\,hv}}$ ($m^2\ m^{-2}\ d^{-1}$). The HPM animal model was not used in any part of this study. The stomatal conductance, g_s ($m\ s^{-1}$), is calculated by a linear function, depending on the relative water content of the shoot, θ_{sh} ($m^3\ m^{-3}$):

$$g_s=\begin{cases}g_{s,\min} & \text{if}\left(\theta\leq\theta_{\mathrm{gs,min}}\ \text{or}\ R_p=0\right)\\ g_{s,\min}+\dfrac{\left(\theta_{\mathrm{sh}}-\theta_{\mathrm{gs,min}}\right)\left(g_{s,\max}-g_{s,\min}\right)}{g_{s,\max}-g_{s.\min}} & \\ & \text{if}\left(\theta_{\mathrm{gs,min}}<\theta_{\mathrm{sh}}\leq\theta_{\mathrm{gs,max}}\ \text{and}\ R_p>0\right)\\ g_{s,\max} & \text{if}\left(\theta_{\mathrm{sh}}\geq\theta_{\mathrm{gs,max}}\ \text{and}\ R_p>0\right)\end{cases} \quad [A18]$$

where g_s is limited by a minimum conductance, $g_{s,\min}$ ($m\ s^{-1}$), and a maximum conductance, $g_{s,\max}$ ($m\ s^{-1}$), which exhibit the corresponding relative shoot water contents $\theta_{\mathrm{gs,min}}$ ($m^3\ m^{-3}$) and $\theta_{\mathrm{gs,max}}$ ($m^3\ m^{-3}$). The equation also depends on the day and night cycles, which are determined by the photosynthetically active radiation R_p ($MJ\ m^{-2}\ d^{-1}$). The HPM assumes that the plant height is proportional to the LAI ($h_{\mathrm{can}} \propto$ LAI). In other words, the harvest management option removes aboveground biomass and decreases the leaf area. Thus, harvest affects the actual transpiration, which significantly changes the latent and sensible heat fluxes.

The root water uptake was computed using the simple Feddes root model (Feddes et al., 2001). In this model, root biomass declines exponentially with rooting depth in the soil profile. The rooting depth of the simulated grasslands was assumed to be constant throughout the simulation period. Dynamic root growth affects energy fluxes due to plant water stress (Gayler et al., 2014), but the root distribution of all species is not known for this site.

Soil Water Flow

The volumetric soil water content, θ_{soil} ($m^3\ m^{-3}$) was simulated with the HYDRUS submodel (Šimůnek et al., 1998):

$$\frac{\partial\theta_{\mathrm{soil}}}{\partial t}=\frac{\partial}{\partial z}K\frac{\partial h}{\partial z}+1-S \quad [A19]$$

where S ($m^3\ m^{-3}\ d^{-1}$) is the loss of soil water due to root water uptake; K ($m\ d^{-1}$) is the soil conductivity; h (m) describes the matric potential in the specific soil layer; t (d) is the time; and z (m) is the soil layer depth. Finite element discretization was used to calculate the water transport. The hydraulic properties were calculated using the van Genuchten–Mualem parameterization of the soil hydraulic properties (van Genuchten, 1980; Mualem, 1976). With the help of the site-specific soil properties (Roth, 2006) and the Rosetta software (Schaap et al., 2001), the van Genuchten parameters for the retention curve were estimated.

Appendix A2: Noah

Noah (Chen and Dudhia, 2001) is a well-established LSM that is implemented in the Weather Research and Forecasting model (Skamarock et al., 2008). A stand-alone one-dimensional version of Noah can be used in an offline mode. This version uses atmospheric forcing at a temporal resolution of 30 min obtained from field measurements of shortwave and longwave radiation, wind speed, temperature, precipitation, relative humidity, and air pressure (Chen et al., 1996b). Noah simulates several biophysical and hydrological processes. These processes control the latent and sensible heat fluxes between the land surface and the atmosphere.

Surface Energy

The computation of the surface energy budget and the net radiation, R ($W\ m^{-2}$), are similar to Expert-N 5.0 Eq. [1] and Eq. [A1], respectively. For more details, see van der Velde et al. (2009). The latent heat, L ($W\ m^{-2}$), is the sum of soil evaporation, E_{dir} ($W\ m^{-2}$), evaporation of precipitation intercepted by the canopy, E_c ($W\ m^{-2}$), and transpiration through the stomata, E_t ($W\ m^{-2}$):

$$L=E_{\mathrm{dir}}+E_c+E_t \quad [A20]$$

The soil evaporation, E_{dir} (W m^{-2}), follows the linear method of Mahfouf and Noilhan (1991):

$$E_{dir} = (1 - f_c)\left(\frac{\theta_{soil,1} - \theta_{soil,dry}}{\theta_{soil,sat} - \theta_{soil,dry}}\right)^2 ET_{pot} \frac{10^6}{3600} \rho_w L_{evap} \quad [A21]$$

where f_c (dimensionless) is the fractional vegetation cover, θ_{soil} (m^3 m^{-3}) is the soil water content, L_{evap} (MJ kg^{-1}) is the latent heat factor, ρ_w (Mg m^{-3}) is the density of water; $10^6/3600$ (h J s^{-1} MJ) is a conversion factor, and ET_{pot} (mm h^{-1}) is the potential evapotranspiration, which is obtained using the Penman-based diurnally dependent potential evaporation approach of Mahrt and Ek (1984). The subscripts *1*, *sat*, and *dry* indicate the soil moisture content of the first soil layer, the saturated soil moisture content, and the wilting point, respectively. The canopy evaporation, E_c (W m^{-2}), is calculated by

$$E_c = f_c ET_{pot} \frac{\left(\theta_{can}/\theta_{can,max}\right)^{0.5} \times 10^6}{3600} \rho_w L_{evap} \quad [A22]$$

where θ_{can} (kg m^{-2}) and $\theta_{can,max}$ (kg m^{-2}) are the actual and maximum canopy moisture contents, respectively. The canopy transpiration, E_t (W m^{-2}), is defined as

$$E_t = f_c P_c ET_{pot} \frac{\left[1 - \left(\theta_{can}/\theta_{can,max}\right)^{0.5}\right] \times 10^6}{3600} \rho_w L_{evap} \quad [A23]$$

where P_c (dimensionless) is the plant coefficient, which depends on wind speed, air temperature, surface pressure, and surface resistance.

The ground heat flux, G (W m^{-2}), is calculated using the temperature gradient between the surface temperature, T_{skin} (K), and the midpoint temperature of the first soil layer, T_{s1} (K), multiplied by the thermal conductivity, κ_t (W m^{-2} K^{-1}):

$$G = \kappa_t \frac{T_{skin} - T_{s1}}{dz} \quad [A24]$$

The value of κ_t is reduced compared with the bare soil κ_t by an exponential function of the LAI. The sensible heat flux, H_s (W m^{-2}), is computed through the application of the bulk transfer relationships (e.g., Garratt (1993)):

$$H_s = \rho_a c_p C_H u_z \left(T_{skin} - \tau_{air}\right) \quad [A25]$$

where ρ_a (kg m^{-3}) is the mean air density, c_p (MJ kg^{-1} K^{-1}) is the specific heat of air, C_H (dimensionless) is the surface exchange coefficient for heat, and τ_{air} (K) is the potential air temperature.

Soil Water Flow

Assuming a homogenous soil profile, the soil water content, θ_{soil} (m^3 m^{-3}), is simulated using the diffusivity form of the Richards equation, which can be formulated as

$$\frac{\partial \theta_{soil}}{\partial t} = \frac{\partial}{\partial z} D \frac{\partial \theta_{soil}}{\partial z} + \frac{\partial \kappa}{\partial z} - S \quad [A26]$$

where κ (m s^{-1}) is the hydraulic conductivity, D (m s^{-1}) is the soil water diffusivity, S (m^3 m^{-3}s) represents sinks and sources, and z (m) is the soil layer depth. The model works with four numerical layers and assumes a constant soil profile (Mahrt and Pan, 1984; Schaake et al., 1996). The relationship between the hydraulic conductivity, κ (m s^{-1}), and the soil water diffusivity, D (m s^{-1}), is defined by the formulation of Cosby et al. (1984) for nine different soil types.

Appendix B: Software Used

- Expert- N, Version 5.0, Rev 605
- Noah, Version 3.4.1 (Chen et al., 1996b, 1997; Chen and Dudhia, 2001; Ek et al., 2003; Koren et al., 1999)
- Rosetta, Version 1.2 (Schaap et al., 2001)
- Matplotlib, Version 1.3.1 (Hunter, 2007)
- NumPy 1.5 (Jones et al., 2001)

Appendix C: Supplemental Material

Ground Heat Flux

Ground heat fluxes are not unimportant for grassland systems compared with forest areas (Park et al., 2011) and cannot be neglected. For example, in tundra regions, G could amount to 25% of R_n during 1986 to 2004 (Park et al., 2008). The comparison of G and R_n from our simulations produced similar results.

The ground heat flux of the five models is presented in Fig. 8. Due to the lack of measurements, the dynamics of ground heat fluxes could only be evaluated by comparisons between the simulations of the different model approaches.

In May during the day, the ground heat flux values of all models were mostly negative and reached values up to −190 W m^{-2} (Fig. 8a). Model I exhibited fluxes of approximately 50 W m^{-2} during the night. No nighttime fluxes were observed in the other models.

In July (dry and hot), the amplitudes of ground heat flux dynamics were significantly lower in simulations by Model III due to the overestimation of the LAI (Fig. 8b). Harvesting had an impact on Models III to V: the minimum daily energy decreased from approximately −50 W m^{-2} to approximately −200 W m^{-2}.

Net Radiation Flux

The net radiation flux of the five models is presented in Fig. 9. In May, the measured diurnal dynamics of the net radiation fluxes were well simulated by all models and did not significantly differ (Fig. 9a).

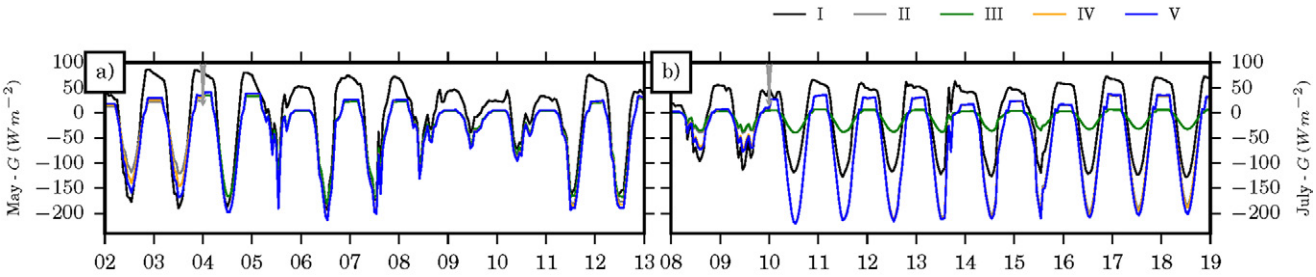

Fig. 8. Simulated (solid lines) dynamics of ground heat flux (G) from (a) 2 to 13 May (temperate, moist) and (b) 8 to 19 July (hot, dry) using Models I (black), II (gray), III (green), IV (orange), and V (blue). Vertical arrows are biomass harvest events.

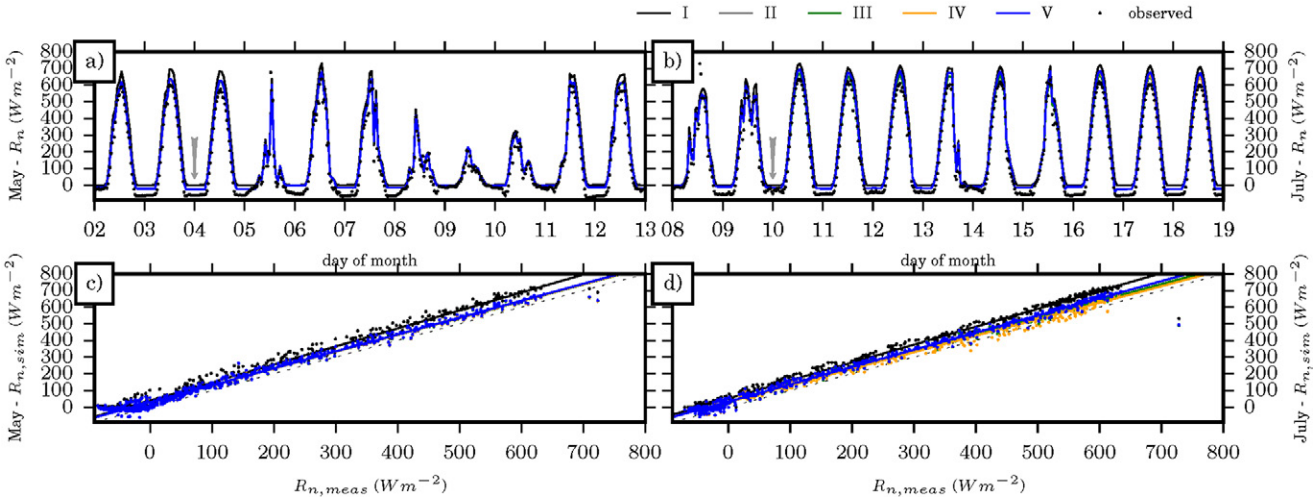

Fig. 9. Measured (dots) and simulated (solid lines) dynamics of net radiation flux (R_n) from (a) 2 to 13 May (temperate, moist) and (b) 8 to 19 July (hot, dry), and (c,d) measured vs. simulated values using Models I (black), II (gray), III (green), IV (orange), and V (blue). Vertical arrows are biomass harvest events.

In the scatterplot (Fig. 9c), the fitted mean lines of all models were parallel to the bisector of the first quadrant. The energies of Models II to V were lower than the simulated values of Model I, but all models overestimated the measured values.

In July (dry and hot), the results were almost identical to the results for May (Fig. 9a and 9b).

Variables and Abbreviations

C_H	surface exchange coefficient for heat
c_p	specific heat of air, MJ kg^{-1} K^{-1}
D	soil water diffusivity, m s^{-1}
d_o	zero plane displacement height, m
e_a	actual vapor pressure, kPa
E_{act}	actual evaporation, mm h^{-1}
E_c	evaporation of precipitation, W m^{-2}
E_{dir}	sum of soil evaporation, W m^{-2}
E_{pot}	potential evaporation, mm h^{-1}
$E_{pot,max}$	maximum of water, which can be evaporated from the soil, mm h^{-1}
e_s	saturated vapor pressure, kPa
E_t	canopy transpiration, W m^{-2}
ET_{act}	actual evapotranspiration, mm h^{-1}
ET_{pot}	potential evapotranspiration, mm h^{-1}
f_c	fractional vegetation cover
f_{cd}	cloudiness factor
f_{lam}	fraction of the leaf area
G	ground heat flux, W m^{-2}
g_s	stomatal conductance, m s^{-1}
$g_{s,max}$	maximum conductance, m s^{-1}
$g_{s,min}$	a minimum conductance, m s^{-1}
G_{sh}	growth rate of the shoot, kg m^{-2} d^{-1}
h	matric potential, m
h_{can}	plant height, m
H_s	sensible heat flux, W m^{-2}
$H_{s,pot}$	W m^{-2}
I^i_{LAI}	LAI input rate, m^2 m^{-2} d^{-1}
k	von Kármán constant
K	soil conductivity, m d^{-1}
k_{can}	leaf extinction coefficient, m^2 m^{-2}

k_{deg}	degradation rate, d^{-1}
k_{turn}	turnover rate, d^{-1}
L	latent heat flux, W m^{-2}
LAI	leaf area index, m^2 m^{-2}
LAI_{act}	active (sunlit) leaf area index, m^2 m^{-2}
L_{evap}	latent heat factor, MJ kg^{-1}
L_{MO}	Obukhov length, m
NSE	Nash–Sutcliffe efficiency
$\bar{O}$	mean observation
O_i	observation value
$O^i_{LAI, an}$	animal grazing rate, m^2 m^{-2} d^{-1}
$O^i_{LAI, hv}$	harvesting rate, m^2 m^{-2} d^{-1}
P_c	plant coefficient
P_i	prediction value
r_a	aerodynamic resistance, s m^{-1}
RMSE	root mean square error
R_n	net amount of radiant energy, W m^{-2}
R_{nl}	net longwave radiation, W m^{-2}
R_{ns}	the non-reflected part of the incoming solar radiation, W m^{-2}
R_p	photosynthetically active radiation, MJ m^{-2} d^{-1}
r_s	surface resistance, s m^{-1}
r_s	plant surface resistance, s m^{-1}
R_s	incoming solar radiation, W m^{-2}
S	loss of soil water due to root water uptake, m^3 m^{-3} d^{-1}
S	sink term, m^3 m^{-3} s
t	time, d
T_{act}	actual transpiration, mm h^{-1}
T_K	surface air temperature, K
T_{pot}	potential transpiration, mm h^{-1}
T_{s1}	mid-point temperature of the first soil layer, K
T_{skin}	surface temperature, K
u_z	wind speed, m s^{-1}
WFPS	water-filled pore space
W_{sh}	maximum of water, which can be transpired from the plant, mm h^{-1}
z_{0h}	roughness length of heat, m
z_{0m}	momentum, m
z_w	height of the wind measurements, m
α	albedo
γ	psychometric constant, kPa K^{-1}
Δ	slope of the saturation vapor pressure temperature curve, kPa K^{-1}
θ_{can}	actual canopy moisture content, kg m^{-2}
$\theta_{can,max}$	maximum canopy moisture content, kg m^{-2}
$\theta_{gs,max}$	maximum relative shoot water contents, m^3 m^{-3}
$\theta_{gs,min}$	minimum relative shoot water contents, m^3 m^{-3}
θ_{sh}	relative shoot water content, m^3 m^{-3}
θ_{soil}	volumetric soil water content, m^3 m^{-3}
$\theta_{soil,1}$	volumetric water content (upper soil)
κ_t	thermal conductivity, W m^{-2} K^{-1}
κ	hydraulic conductivity, m s^{-1}
ν	specific leaf area, m^2 kg^{-1}
ρ_a	actual vapor pressure, kg m^{-3}
ρ_w	density of water, Mg m^{-3}
σ	Stefan-Boltzmann constant, W K^{-4} m^{-2}
τ_{air}	potential air temperature, K
Ψ_h	stability function
Ψ_m	stability function

Acknowledgments

We gratefully acknowledge the support of TERENO (Terrestrial Environmental Observatories) funded by the Helmholtz-Gemeinschaft; C. Biernath, C. Klein, and C. Thieme were funded by the Helmholtz project "REKLIM- Regional Climate Change"; F. Heinlein was funded by the German Research Foundation (Deutsche Forschungsgemeinschaft, DFG) under Grant FOR1695; A.K. Gilgen acknowledges the NCCR Climate. This work is a contribution to the Helmholtz Climate Initiative REKLIM (Regional Climate Change), a joint research project of the Helmholtz Association of German Research Centers (HGF). This work used eddy covariance data acquired by the FLUXNET community and in particular by the following networks: CarboExtreme (EU-FP7) and GHG-Europe (EU-FP7).

References

Allen, R.G. 2005. The ASCE standardized reference evapotranspiration equation. Am. Soc. Civ. Eng., Reston, VA.

Allen, R., W. Pruitt, J. Wright, T. Howell, F. Ventura, R. Snyder, et al. 2006. A recommendation on standardized surface resistance for hourly calculation of reference ET_o by the FAO56 Penman–Monteith method. Agric. Water Manage. 81:1–22. doi:10.1016/j.agwat.2005.03.007

Alt, C. 2000. Modelling nitrogen content and distribution in cauliflower (*Brassica oleracea* L. *botrytis*). Ann. Bot. 86:963–973. doi:10.1006/anbo.2000.1252

Ammann, C., C. Flechard, J. Leifeld, A. Neftel, and J. Fuhrer. 2007. The carbon budget of newly established temperate grassland depends on management intensity. Agric. Ecosyst. Environ. 121:5–20. doi:10.1016/j.agee.2006.12.002

Amthor, J. 2000. The McCree–de Wit–Penning de Vries–Thornley respiration paradigms: 30 years later. Ann. Bot. 86:1–20. doi:10.1006/anbo.2000.1175

Asseng, S., F. Ewert, C. Rosenzweig, J.W. Jones, J.L. Hatfield, A.C. Ruane, et al. 2013. Uncertainty in simulating wheat yields under climate change. Nat. Clim. Change 3:827–832. doi:10.1038/nclimate1916

Biernath, C., S. Gayler, S. Bittner, C. Klein, P. Högy, A. Fangmeier, and E. Priesack. 2011. Evaluating the ability of four crop models to predict different environmental impacts on spring wheat grown in open-top chambers. Eur. J. Agron. 35:71–82. doi:10.1016/j.eja.2011.04.001

Bondeau, A., P.C. Smith, S. Zaehle, S. Schaphoff, W. Lucht, W. Cramer, et al. 2007. Modelling the role of agriculture for the 20th century global terrestrial carbon balance. Global Change Biol. 13:679–706. doi:10.1111/j.1365-2486.2006.01305.x

Brisson, N., C. Gary, E. Justes, R. Roche, B. Mary, D. Ripoche, et al. 2003. An overview of the crop model STICS. Eur. J. Agron. 18:309–332. doi:10.1016/S1161-0301(02)00110-7

Brown, R.N., C. Percivalle, S. Narkiewicz, and S. DeCullo. 2010. Relative rooting depths of native grasses and amenity grasses with potential for use on roadsides in New England. HortScience 45:393–400.

Brunt, D. 1932. Notes on radiation in the atmosphere: I. Q. J. R. Meteorol. Soc. 58:389–420. doi:10.1002/qj.49705824704

Brunt, D. (1954) 2011. Physical and dynamical meteorology. Cambridge Univ. Press, New York.

Brutsaert, W. 1982. Evaporation into the atmosphere: Theory, history, and applications. Springer, Dordrecht, the Netherlands. doi:10.1007/978-94-017-1497-6.

Calanca, P., C. Deléglise, R. Martin, P. Carrère, and E. Mosimann. 2016. Testing the ability of a simple grassland model to simulate the seasonal effects of drought on herbage growth. Field Crops Res. 187:12–23. doi:10.1016/j.fcr.2015.12.008

Casanova, J.J., and J. Judge. 2008. Estimation of energy and moisture

fluxes for dynamic vegetation using coupled SVAT and crop-growth models. Water Resour. Res. 44:W07415. doi:10.1029/2007WR006503.

Chang, J., P. Ciais, N. Viovy, N. Vuichard, M. Herrero, P. Havlík, et al. 2015. Effect of climate change, CO_2 trends, nitrogen addition, and land-cover and management intensity changes on the carbon balance of European grasslands. Global Change Biol. 22:338–350. doi:10.1111/gcb.13050

Chang, J.F., N. Viovy, N. Vuichard, P. Ciais, T. Wang, A. Cozic, et al. 2013. Incorporating grassland management in ORCHIDEE: Model description and evaluation at 11 eddy-covariance sites in Europe. Geosci. Model Dev. 6:2165–2181. doi:10.5194/gmd-6-2165-2013

Chaves, M.M. 2002. How plants cope with water stress in the field? Photosynthesis and growth. Ann. Bot. 89:907–916. doi:10.1093/aob/mcf105

Chen, D.-X., H. Hunt, and J. Morgan. 1996a. Responses of a C_3 and C_4 perennial grass to CO_2 enrichment and climate change: Comparison between model predictions and experimental data. Ecol. Modell. 87:11–27. doi:10.1016/0304-3800(94)00199-5

Chen, F., and J. Dudhia. 2001. Coupling an advanced land surface–hydrology model with the Penn State–NCAR MM5 modeling system: I. Model implementation and sensitivity. Mon. Weather Rev. 129:569–585. doi:10.1175/1520-0493(2001)129<0569:CAALSH>2.0.CO;2

Chen, F., Z. Janjić, and K. Mitchell. 1997. Impact of atmospheric surface-layer parameterizations in the new land-surface scheme of the NCEP mesoscale Eta model. Boundary-Layer Meteorol. 85:391–421. doi:10.1023/A:1000531001463

Chen, F., K. Mitchell, J. Schaake, Y. Xue, H.L. Pan, V. Koren, et al. 1996b. Modeling of land surface evaporation by four schemes and comparison with FIFE observations. J. Geophys. Res. 101:7251–7268. doi:10.1029/95JD02165

Chen, S., J. Chen, G. Lin, W. Zhang, H. Miao, L. Wei, et al. 2009. Energy balance and partition in Inner Mongolia steppe ecosystems with different land use types. Agric. For. Meteorol. 149:1800–1809. doi:10.1016/j.agrformet.2009.06.009

Chenge, Y., and W. Brutsaert. 2005. Flux-profile relationships for wind speed and temperature in the stable atmospheric boundary layer. Boundary-Layer Meteorol. 114:519–538. doi:10.1007/s10546-004-1425-4

Choudhury, B. 1989. Estimating evaporation and carbon assimilation using infrared temperature data: Vistas in modeling. In: G. Asrar, editor, Theory and applications of optical remote sensing. John Wiley & Sons, New York. p. 628–690.

Choudhury, B., S. Idso, and R. Reginato. 1987. Analysis of an empirical model for soil heat flux under a growing wheat crop for estimating evaporation by an infrared-temperature based energy balance equation. Agric. For. Meteorol. 39:283–297. doi:10.1016/0168-1923(87)90021-9

Clouaire, R.M., and J.P. Rellier. 2009. Modelling and simulating work practices in agriculture. Int. J. Metadata Semant. Ontol. 4:42–53. doi:10.1504/IJMSO.2009.026253

Cosby, B.J., G.M. Hornberger, R.B. Clapp, and T.R. Ginn. 1984. A statistical exploration of the relationships of soil moisture characteristics to the physical properties of soils. Water Resour. Res. 20:682–690. doi:10.1029/WR020i006p00682

Dierschke, H., and G. Briemle. 2002. Kulturgrasland. Wiesen, Weiden und verwandte Staudenfluren. Ulmer, Stuttgart, Germany.

Donnelly, J., M. Freer, L. Salmon, A. Moore, R. Simpson, H. Dove, and T. Bolger. 2002. Evolution of the GRAZPLAN decision support tools and adoption by the grazing industry in temperate Australia. Agric. Syst. 74:115–139. doi:10.1016/S0308-521X(02)00024-0

Ek, M.B., K.E. Mitchell, Y. Lin, E. Rogers, P. Grunmann, V. Koren, et al. 2003. Implementation of Noah land surface model advances in the National Centers for Environmental Prediction operational mesoscale Eta model. J. Geophys. Res. 108. doi:10.1029/2002JD003296

Ershadi, A., M. McCabe, J. Evans, N. Chaney, and E. Wood. 2014. Multi-site evaluation of terrestrial evaporation models using FLUXNET data. Agric. For. Meteorol. 187:46–61. doi:10.1016/j.agrformet.2013.11.008

Fader, M., W. von Bloh, S. Shi, A. Bondeau, and W. Cramer. 2015. Modelling Mediterranean agro-ecosystems by including agricultural trees in the LPJmL model. Geosci. Model Dev. 8:3545–3561. doi:10.5194/gmd-8-3545-2015

Falge, E., S. Reth, N. Brüggemann, K. Butterbach-Bahl, V. Goldberg, A. Oltchev, et al. 2005. Comparison of surface energy exchange models with eddy flux data in forest and grassland ecosystems of Germany. Ecol. Modell. 188:174–216. doi:10.1016/j.ecolmodel.2005.01.057

FAO. 2015. Status of the world's soil resources. Main report. FAO, Rome.

Fatichi, S., M.J. Zeeman, J. Fuhrer, and P. Burlando. 2014. Ecohydrological effects of management on subalpine grasslands: From local to catchment scale. Water Resour. Res. 50:148–164. doi:10.1002/2013WR014535

Feddes, R., H. Hoff, M. Bruen, T. Dawson, P. de Rosnay, P. Dirmeyer, et al. 2001. Modeling root water uptake in hydrological and climate models. Bull. Am. Meteor. Soc. 82:2797–2809. doi:10.1175/1520-0477(2001)082<2797:MRWUIH>2.3.CO;2

Fiala, K. 2010. Belowground plant biomass of grassland ecosystems and its variation according to ecological factors. Ekologia 29:182–206. doi:10.4149/ekol_2010_02_182

Garratt, J. 1993. Sensitivity of climate simulations to land-surface and atmospheric boundary-layer treatments: A review. J. Clim. 6:419–448. doi:10.1175/1520-0442(1993)006<0419:SOCSTL >2.0.CO;2

Gayler, S., T. Wöhling, M. Grzeschik, J. Ingwersen, H.D. Wizemann, K. Warrach-Sagi, et al. 2014. Incorporating dynamic root growth enhances the performance of Noah-MP at two contrasting winter wheat field sites. Water Resour. Res. 50:1337–1356. doi:10.1002/2013WR014634

Gigante, V., V. Iacobellis, S. Manfreda, P. Milella, and I. Portoghese. 2009. Influences of leaf area index estimations on water balance modeling in a Mediterranean semi-arid basin. Nat. Hazards Earth Syst. Sci. 9:979–991. doi:10.5194/nhess-9-979-2009

Gilgen, A.K., and N. Buchmann. 2009. Response of temperate grasslands at different altitudes to simulated summer drought differed but scaled with annual precipitation. Biogeosciences 6:2525–2539. doi:10.5194/bg-6-2525-2009

Gilgen, A.K., C. Signarbieux, U. Feller, and N. Buchmann. 2010. Competitive advantage of *Rumex obtusifolius* L. might increase in intensively managed temperate grasslands under drier climate. Agric. Ecosyst. Environ. 135:15–23. doi:10.1016/j.agee.2009.08.004

Hansen, S., H. Jensen, N. Nielsen, and H. Svendsen. 1991. Simulation of nitrogen dynamics and biomass production in winter wheat using the Danish simulation model DAISY. Nutr. Cycling Agroecosyst. 27:245–259. doi:10.1007/BF01051131

Herndl, M., M. Kandolf, A. Bohner, B. Krautzer, W. Graiss, and M. Schink. 2011. Wurzelparameter von Gräsern, Kräutern und Leguminosen als Grundlage zur Bewertung von Trockenheitstoleranz im Grünland. In: 1st Tagung der Österreichischen Gesellschaft für Wurzelforschung, Irdning, Austria. 13–14 Sept. 2011. Forschungszentrum für Landwirtschaft Raumberg-Gumpenstein, Irdning-Donnersbachtal, Austria. p. 45–54.

Hidy, D., Z. Barcza, L. Haszpra, G. Churkina, K. Pintér, and Z. Nagy. 2012. Development of the Biome-BGC model for simulation of managed herbaceous ecosystems. Ecol. Modell. 226:99–119. doi:10.1016/j.ecolmodel.2011.11.008

Holzworth, D.P., N.I. Huth, P.G. deVoil, E.J. Zurcher, N.I. Herrmann, G. McLean, et al. 2014. APSIM: Evolution towards a new generation of agricultural systems simulation. Environ. Model. Softw. 62:327–350. doi:10.1016/j.envsoft.2014.07.009

Hunter, J.D. 2007. Matplotlib: A 2D graphics environment. Comput. Sci. Eng. 9:90–95. doi:10.1109/MCSE.2007.55

Hurtado-Uria, C., D. Hennessy, L. Shalloo, R.P.O. Schulte, L. Delaby, and D. O'Connor. 2012. Evaluation of three grass growth models to predict grass growth in Ireland. J. Agric. Sci. 151:91–104. doi:10.1017/S0021859612000317

Hutchings, N., J. Olesen, B. Petersen, and J. Berntsen. 2007. Modelling spatial heterogeneity in grazed grassland and its effects on nitrogen cycling and greenhouse gas emissions. Agric. Ecosyst. Environ. 121:153–163. doi:10.1016/j.agee.2006.12.009

Hutson, J., and R. Wagenet. 1992. LEACHM: Leaching estimation and chemistry model: A process-based model of water and solute movement, transformations, plant uptake and chemical reactions in the unsaturated zone. Version 3.0. Res. Ser. 93-3. Dep. of Soil, Crop and Atmospheric Sciences, Cornell Univ., Ithaca, NY.

Johnson, I. 2013. Dairymod and the SGS pasture model: A mathematical description of the biophysical model structure. IMJ Consultants, Dorrigo, NSW, Australia.

Jones, E., T. Oliphant, P. Peterson, et al. 2001. SciPy: Open source scientific tools for Python. http://www.scipy.org/ (accessed 16 Aug. 2014).

Jones, J., G. Hoogenboom, C. Porter, K. Boote, W. Batchelor, L. Hunt, et al. 2003. The DSSAT cropping system model. Eur. J. Agron. 18:235–265. doi:10.1016/S1161-0301(02)00107-7

Kalapos, T., R. van den Boogaard, and H. Lambers. 1996. Effect of soil drying on growth, biomass allocation and leaf gas exchange of two annual grass species. Plant Soil 185:137–149. doi:10.1007/BF02257570

Keller, E.D., W.T. Baisden, L. Timar, B. Mullan, and A. Clark. 2014. Grassland production under global change scenarios for New Zealand pastoral agriculture. Geosci. Model Dev. 7:2359–2391. doi:10.5194/gmd-7-2359-2014

Kelliher, F., R. Leuning, M. Raupach, and E.D. Schulze. 1995. Maximum

conductances for evaporation from global vegetation types. Agric. For. Meteorol. 73:1–16. doi:10.1016/0168-1923(94)02178-M

Kirschbaum, M.U., S. Rutledge, I.A. Kuijper, P.L. Mudge, N. Puche, A.M. Wall, et al. 2015. Modelling carbon and water exchange of a grazed pasture in New Zealand constrained by eddy covariance measurements. Sci. Total Environ. 512–513:273–286. doi:10.1016/j.scitotenv.2015.01.045

Koren, V., J. Schaake, K. Mitchell, Q.Y. Duan, F. Chen, and J.M. Baker. 1999. A parameterization of snowpack and frozen ground intended for NCEP weather and climate models. J. Geophys. Res. 104:19569–19585. doi:10.1029/1999JD900232

Körner, C. 2003. Alpine plant life: Functional plant ecology of high mountain ecosystems. 2nd ed. Springer, Berlin. doi:10.1007/978-3-642-18970-8

Li, C., S. Frolking, and T.A. Frolking. 1992. A model of nitrous oxide evolution from soil driven by rainfall events: 1. Model structure and sensitivity. J. Geophys. Res. 97:9759–9776. doi:10.1029/92JD00509

Li, C., S. Frolking, and R. Harriss. 1994. Modeling carbon biogeochemistry in agricultural soils. Global Biogeochem. Cycles 8:237–254. doi:10.1029/94GB00767

Lin, T.S., and F.Y. Cheng. 2016. Impact of soil moisture initialization and soil texture on simulated land–atmosphere interaction in Taiwan. J. Hydrometeorol. 17:1337–1355. doi:10.1175/JHM-D-15-0024.1

Ma, S., R. Lardy, A.I. Graux, H.B. Touhami, K. Klumpp, R. Martin, and G. Bellocchi. 2015. Regional-scale analysis of carbon and water cycles on managed grassland systems. Environ. Modell. Softw. 72:356–371. doi:10.1016/j.envsoft.2015.03.007

Mahfouf, J., and J. Noilhan. 1991. Comparative study of various formulations of evaporations from bare soil using in situ data. J. Appl. Meteorol. 30:1354–1365. doi:10.1175/1520-0450(1991)030<1354:CSOVFO>2.0.CO;2

Mahmood, R., and K.G. Hubbard. 2003. Simulating sensitivity of soil moisture and evapotranspiration under heterogeneous soils and land uses. J. Hydrol. 280:72–90. doi:10.1016/s0022-1694(03)00183-5

Mahrt, L., and M. Ek. 1984. The influence of atmospheric stability on potential evaporation. J. Climate Appl. Meteor. 23:222–234. doi:10.1175/1520-0450(1984)023<0222:TIOASO>2.0.CO;2

Mahrt, L., and H. Pan. 1984. A two-layer model of soil hydrology. Boundary-Layer Meteor. 29:1–20. doi:10.1007/bf00119116

Mariotte, P., C. Vandenberghe, P. Kardol, F. Hagedorn, and A. Buttler. 2013. Subordinate plant species enhance community resistance against drought in semi-natural grasslands. J. Ecol. 101:763–773. doi:10.1111/1365-2745.12064

Miller, D., and R. White. 1998. A conterminous United States multilayer soil characteristics dataset for regional climate and hydrology modeling. Earth Interact. 2:1–26. doi:10.1175/1087-3562(1998)002<0001:ACUSMS>2.3.CO;2

Monteith, J. 1965. Evaporation and environment. Symp. Soc. Exp. Biol. 19:205–234.

Monteith, J. 1981. Evaporation and surface temperature. Q. J. R. Meteorol. Soc. 107:1–27. doi:10.1002/qj.49710745102

Monteith, J. 1991. Plant and crop modelling: A mathematical approach to plant and crop physiology. Agric. Syst. 37:451–452. doi:10.1016/0308-521X(91)90064-H

Monteith, J.L. 1993. Plants and microclimate. 2nd ed. Cambridge Univ. Press, Cambridge, UK.

Mualem, Y. 1976. A new model for predicting the hydraulic conductivity of unsaturated porous media. Water Resour. Res. 12:513–522. doi:10.1029/WR012i003p00513

Nash, J., and J. Sutcliffe. 1970. River flow forecasting through conceptual models: I. A discussion of principles. J. Hydrol. 10:282–290. doi:10.1016/0022-1694(70)90255-6

Pan, H.L., and L. Mahrt. 1987. Interaction between soil hydrology and boundary-layer development. Boundary-Layer Meteorol. 38:185–202. doi:10.1007/BF00121563

Park, H., T. Yamazaki, and T. Oht. 2011. Responses of energy budget and evapotranspiration to climate change in eastern Siberia. In: L. Labedzki, editor, Evapotranspiration. InTech, London. doi:10.5772/14161

Park, H., T. Yamazaki, K. Yamamoto, and T. Ohta. 2008. Tempo-spatial characteristics of energy budget and evapotranspiration in the eastern Siberia. Agric. For. Meteorol. 148:1990–2005. doi:10.1016/j.agrformet.2008.06.018

Parton, W., M. Hartman, D. Ojima, and D. Schimel. 1998. DAYCENT and its land surface submodel: Description and testing. Global Planet. Change 19:35–48. doi:10.1016/S0921-8181(98)00040-X

Peuke, A.D., J. Glaab, W.M. Kaiser, and W.D. Jeschke. 1996. The uptake and flow of C, N and ions between roots and shoots in *Ricinus communis* L.: IV. Flow and metabolism of inorganic nitrogen and malate depending on nitrogen nutrition and salt treatment. J. Exp. Bot. 47:377–385. doi:10.1093/jxb/47.3.377

Prechsl, U.E., S. Burri, A.K. Gilgen, A. Kahmen, and N. Buchmann. 2014. No shift to a deeper water uptake depth in response to summer drought of two lowland and sub-alpine C_3-grasslands in Switzerland. Oecologia 177:97–111. doi:10.1007/s00442-014-3092-6

Priesack, E. 2006. Expert-N Dokumentation der Modellbibliothek- FAM-Bericht 60. Forschungsverbund Agrarökosysteme München-Erfassung, Prognose und Bewertung nutzungsbedingter Veränderungen in Agrarökosystemen und deren Umwelt. Hyronimus, München, Germany.

Priesack, E., S. Gayler, and H.P. Hartmann. 2006. The impact of crop growth sub-model choice on simulated water and nitrogen balances. Nutr. Cycling Agroecosyst. 75:1–13. doi:10.1007/s10705-006-9006-1

Raes, D., P. Van Aelst, and G. Wyseure. 1986. ETref, ETcrop, ETsplit and deficit, a computer package for calculating crop water requirements: Reference manual. Lab. of Soil and Water Eng., Leuven, Belgium.

Riedo, M., A. Grub, M. Rosset, and J. Fuhrer. 1998. A pasture simulation model for dry matter production, and fluxes of carbon, nitrogen, water and energy. Ecol. Modell. 105:141–183. doi:10.1016/S0304-3800(97)00110-5

Robson, M.J. 1973. The growth and development of simulated swards of perennial ryegrass: I. leaf growth and dry weight change as related to the ceiling yield of a seedling sward. Ann. Bot. 37:487–500. doi:10.1093/oxfordjournals.aob.a084716

Roth, K. 2006. Bodenkartierung und GIS-basierte Kohlenstoffinventur von Graslandböden: Untersuchungen an den ETH- Forschungsstationen Chamau und Früebüel (ZG, Schweiz). M.S. thesis. Dep. of Geogr., Univ. of Zurich.

Rotz, C.A., B.J. Isenberg, K.R. Stackhouse-Lawson, and E.J. Pollak. 2013. A simulation-based approach for evaluating and comparing the environmental footprints of beef production systems. J. Anim. Sci. 91:5427–5437. doi:10.2527/jas.2013-6506

Ruget, F., S. Satger, F. Volaire, and F. Lelièvre. 2009. Modeling tiller density, growth, and yield of Mediterranean perennial grasslands with STICS. Crop Sci. 49:2379. doi:10.2135/cropsci2009.06.0323

Schaake, J.C., V.I. Koren, Q.Y. Duan, K. Mitchell, and F. Chen. 1996. Simple water balance model for estimating runoff at different spatial and temporal scales. J. Geophys. Res. 101:7461–7475. doi:10.1029/95JD02892

Schaap, M.G., F.J. Leij, and M.Th. van Genuchten. 2001. Rosetta: A computer program for estimating soil hydraulic parameters with hierarchical pedotransfer functions. J. Hydrol. 251:163–176. doi:10.1016/S0022-1694(01)00466-8

Schapendonk, A., W. Stol, D. van Kraalingen, and B. Bouman. 1998. LINGRA, a sink/source model to simulate grassland productivity in Europe. Eur. J. Agron. 9:87–100. doi:10.1016/S1161-0301(98)00027-6

Schulze, E.D. 1994. Relationships among maximum stomatal conductance, ecosystem surface conductance, carbon assimilation rate, and plant nitrogen nutrition: A global ecology scaling exercise. Annu. Rev. Ecol. Syst. 25:629–662. doi:10.1146/annurev.es.25.110194.003213

Senapati, N., P.E. Jansson, P. Smith, and A. Chabbi. 2016. Modelling heat, water and carbon fluxes in mown grassland under multi-objective and multi-criteria constraints. Environ. Modell. Softw. 80:201–224. doi:10.1016/j.envsoft.2016.02.025

Silva, J., J. Toland, W. Jones, J. Eldridge, E. Thorpe, and E. O'Hara. 2008. LIFE and Europe's grasslands: Restoring a forgotten habitat. Publications Office of the European Union, Luxembourg. doi:10.2779/23028

Šimůnek, J., K. Huang, and M.Th. van Genuchten. 1998. The HYDRUS code for simulating the one-dimensional movement of water, heat, and multiple solutes in variably-saturated media. Version 6.0. Univ. of California, Riverside.

Sindhøj, E., A.-C. Hansson, O. Andrén, T. Kätterer, M. Marissink, and R. Pettersson. 2000. Root dynamics in a semi-natural grassland in relation to atmospheric carbon dioxide enrichment, soil water and shoot biomass. Plant Soil 223:255–265. doi:10.1023/A:1004801718567

Skamarock, W., J. Klemp, J. Dudhia, D. Gill, D. Barker, M. Duda, et al. 2008. A description of the advanced research WRF version 3. NCAR Tech. Note NCAR/TN-475+STR. Natl. Ctr. Atmos. Res., Boulder, CO. doi:10.5065/D68S4MVH

Snow, V., C. Rotz, A. Moore, R. Martin-Clouaire, I. Johnson, N. Hutchings, and R. Eckard. 2014. The challenges—and some solutions—to process-based modelling of grazed agricultural systems. Environ. Modell. Softw. 62:420–436. doi:10.1016/j.envsoft.2014.03.009

Song, Y., A.K. Jain, and G.F. McIsaac. 2013. Implementation of dynamic crop growth processes into a land surface model: Evaluation of energy, water and carbon fluxes under corn and soybean rotation. Biogeosciences 10:8039–8066. doi:10.5194/bg-10-8039-2013

Stöckle, C.O., M. Donatelli, and R. Nelson. 2003. CropSyst, a crop-

ping systems simulation model. Eur. J. Agron. 18:289–307. doi:10.1016/S1161-0301(02)00109-0

Strengers, B.J., C. Müller, M. Schaeffer, R.J. Haarsma, C. Severijns, D. Gerten, et al. 2010. Assessing 20th century climate–vegetation feedbacks of land-use change and natural vegetation dynamics in a fully coupled vegetation–climate model. Int. J. Climatol. 30:2055–2065. doi:10.1002/joc.2132

Thomas, H., M.B. Jones, and A. Lazenby. 1989. The grass crop: The physiological basis of production. J. Appl. Ecol. 26:1095. doi:10.2307/2403725

Thornley, J. 1998. Grassland dynamics: An ecosystem simulation model. CAB Int., Wallingford, UK.

Thornley, J. 2001. Simulating grass–legume dynamics: A phenomenological submodel. Ann. Bot. 88:905–913. doi:10.1006/anbo.2001.1529

Thornley, J., and M. Cannell. 1997. Temperate grassland responses to climate change: An analysis using the Hurley Pasture Model. Ann. Bot. 80:205. doi:10.1006/anbo.1997.0430

Tsarouchi, G.M., W. Buytaert, and A. Mijic. 2014. Coupling a land-surface model with a crop growth model to improve ET flux estimations in the Upper Ganges basin, India. Hydrol. Earth Syst. Sci. 18:4223–4238. doi:10.5194/hess-18-4223-2014

Van den Hoof, C., E. Hanert, and P.L. Vidale. 2011. Simulating dynamic crop growth with an adapted land surface model—JULES-SUCROS: Model development and validation. Agric. For. Meteorol. 151:137–153. doi:10.1016/j.agrformet.2010.09.011

van der Velde, R., Z. Su, M. Ek, M. Rodell, and Y. Ma. 2009. Influence of thermodynamic soil and vegetation parameterizations on the simulation of soil temperature states and surface fluxes by the Noah LSM over a Tibetan plateau site. Hydrol. Earth Syst. Sci. 13:759–777. doi:10.5194/hess-13-759-2009

van Genuchten, M.Th. 1980. A closed-form equation for predicting the hydraulic conductivity of unsaturated soils. Soil Sci. Soc. Am. J. 44:892–898. doi:10.2136/sssaj1980.03615995004400050002x

van Wijk, M.T. 2010. Understanding plant rooting patterns in semi-arid systems: An integrated model analysis of climate, soil type and plant biomass. Global Ecol. Biogeogr. 20:331–342. doi:10.1111/j.1466-8238.2010.00601.x

Volaire, F. 2008. Plant traits and functional types to characterise drought survival of pluri-specific perennial herbaceous swards in Mediterranean areas. Eur. J. Agron. 29:116–124. doi:10.1016/j.eja.2008.04.008

Volaire, F., and F. Lelièvre. 2001. Drought survival in *Dactylis glomerata* and *Festuca arundinacea* under similar rooting conditions in tubes. Plant Soil 229:225–234. doi:10.1023/A:1004835116453

Walter, J., K. Grant, C. Beierkuhnlein, J. Kreyling, M. Weber, and A. Jentsch. 2012. Increased rainfall variability reduces biomass and forage quality of temperate grassland largely independent of mowing frequency. Agric. Ecosyst. Environ. 148:1–10. doi:10.1016/j.agee.2011.11.015

Williams, J.R., C.A. Jones, J.R. Kiniry, and D.A. Spanel. 1989. The EPIC crop growth model. Trans. ASAE 32:497–511. doi:10.13031/2013.31032

Williams, K.E., and P.D. Falloon. 2015. Sources of interannual yield variability in JULES-crop and implications for forcing with seasonal weather forecasts. Geosci. Model Dev. 8:3987–3997. doi:10.5194/gmd-8-3987-2015

Zeeman, M., R. Hiller, A.K. Gilgen, P. Michna, P. Plüss, N. Buchmann, and W. Eugster. 2010. Management and climate impacts on net CO_2 fluxes and carbon budgets of three grasslands along an elevational gradient in Switzerland. Agric. For. Meteorol. 150:519–530. doi:10.1016/j.agrformet.2010.01.011